International Journal of Energy and Environmental Engineering (2018) 9:473–498
https://doi.org/10.1007/s40095-018-0276-6

ORIGINAL RESEARCH

Effect of cooling condensing cover on the performance of *N*-identical photovoltaic thermal-compound parabolic concentrator active solar still: a comparative study

Poonam Joshi[1] · **G. N. Tiwari**[2]

Received: 30 November 2017 / Accepted: 30 May 2018 / Published online: 21 June 2018

Abstract

In this work, photovoltaic thermal-compound parabolic concentrators (PVT-CPC) are integrated to a single slope solar still (SS-SS) through a heat exchanger placed in the basin. A continuous water flow is provided over the condensing cover of SS-SS for yield enhancement. An effect of cooling condensing cover on energy and exergy analysis (thermal and electrical) together with the production cost of distilled water (₹/kg) has been studied for the following three cases: (I) the proposed partially covered photovoltaic thermal-compound parabolic concentrator single slope solar still (PVT-CPC-SS-SS), (II) fully covered thermal-compound parabolic concentrator single slope solar still (PVT-CPC-SS-SS), and (III) flat plate thermal-compound parabolic concentrator single slope solar still (FPC-CPC-SS-SS). Design parameters have been optimized for maximum distillate output (energy) and exergy on annual performance basis. Moreover, higher daily yield (37.9 kg) is obtained for case (iii). In addition, higher electrical module efficiency (13%) is obtained for case (ii) for the month of January when the solar cell temperature is 55 °C at the optimized conditions. However, the proposed system gives daily yield (35.78 kg) and generates electricity at module efficiency of 12%. The energy payback time of the proposed system is estimated to be 2 years.

Keywords Photovoltaic thermal-compound parabolic concentrator (PVT-CPC) · Solar distillation · Heat exchanger · Energy and exergy

List of symbols

A	Area (m^2)
A_m	Module area (m^2)
A_g	Area of glass (m^2)
A_b	Area of basin (m^2)
C_f	Specific heat capacity of fluid (water) $\left(\frac{J}{kg\ K}\right)$
C_w	Specific heat capacity of water $\left(\frac{J}{kg\ K}\right)$
dx	Elemental section
g	Acceleration due to gravity
Gr	Grashof Number
E_x	Exergy
h_{rw}	Radiative heat transfer coefficient ($W/m^2\ K$)
h_{cw}	Convective heat transfer coefficient ($W/m^2\ K$)
h_{ew}	Evaporative heat transfer coefficient ($W/m^2\ K$)
h_{bw}	Heat transfer coefficient from basin to water (W/m^2K)
h_{ba}	Heat transfer coefficient from basin to ambient ($W/m^2\ K$)
$I(t)$	Solar radiation (W/m^2)
K_g	Thermal conductivity $\left(\frac{W}{m}K\right)$
L_g	Length of glass (m)
$\dot{m}_f$	Mass flow rate of working fluid (kg/s)
N	Number of thermal collectors
Nu	Nusselt number
Pr	Prandlt number
P_w	Partial saturated water vapor at water temperature $\left(\frac{N}{m^2}\right)$
P_{gi}	Partial saturated water vapor at glass temperature $\left(\frac{N}{m^2}\right)$

Electronic supplementary material The online version of this article (https://doi.org/10.1007/s40095-018-0276-6) contains supplementary material, which is available to authorized users.

✉ Poonam Joshi
poonam_joshi@aol.com; pjoshi3112@gmail.com

[1] Centre for Energy Studies, Indian Institute of Technology Delhi, Delhi, India

[2] Bag Energy Research Society (BERS), SODHA BERS COMPLEX, Plot No. 51, Mahamana Nagar, Karaudi, Varanasi, UP 22 10 05, India

$\dot{Q}_{u,N}$	Rate of useful energy (W)
r_1	Inner radius of heat exchanger (m)
r_2	Outer radius of heat exchanger (m)
t	Time
T	Temperature (°C)
T_a	Ambient temperature (°C)
T_{foN}	Outlet fluid temperature (°C)
T_w	Water temperature (°C)
T_{wf}	Temperature of water flowing above condensing cover (°C)
T_{fi}	Inlet water temperature (°C)
T_{gi}	Inner glass temperature (°C)
T_{go}	Outer glass temperature (°C)
U	Overall heat transfer coefficient (W/m^2 K)

Subscript

a	Ambient air
eff	Effective
g	Glass
w	Water

Greek letters

α	Absorptivity
α_b	Absorptivity of basin
α_w	Absorptivity of water
$(\alpha\tau)_{eff}$	Product of effective absorptivity and
τ	Transmissivity
η_m	Module efficiency

Introduction

Water is crucial to sustain life on earth, and its demand is primarily influenced by climate change, population growth and urbanization, and energy security policies. Last few decades have seen a sharp decline in the availability of potable water and it is projected that the world will face a 20% water deficit by 2030 [1]. World Health Organization (WHO), World Bank (WB), World Wildlife Fund (WWF), World Water Council (WWC), United Nation Development Program (UNDP), etc., have worked extensively to promote water conservation by regulation and implementation of water policies. This clearly indicates that access to potable water continues to be a major problem.

To address the global crisis of water availability, solar desalination/distillation promises to be an effective technology. Solar still (passive/active) harness solar energy (emission free), which distillates brackish water (≈10,000) ppm and saline water (≈45,000) ppm into potable water. A first solar distillation apparatus was described by Giovanni Battista Della Porta (1535–1615) [2]. After him many researchers worked on different designs (Table 1) of a solar still to improve the performance of the system on an hourly and annual basis to obtain the increased quantity of potable water. However, the performance of a solar still is limited by the temperature difference (ΔT) between condensing and evaporating areas. A continuous flow of water or air over condensing cover leads to cooling, which increases the temperature difference and improves productivity (Table 1). In addition, it cleans the dirt and filth on the condensing cover, which otherwise, reduces the solar still (SS) efficiency. Table 1 also includes previous work done for the increase in yield, efficiency, and productivity of a solar still because of cooling the condensing cover.

Previous studies (Table 1) on passive and active solar stills show that active solar still have higher productivity as they are integrated to external heat sources, e.g., flat plate collector, evacuated tubular collector, solar concentrators, photovoltaic thermal flat plate collector, and photovoltaic thermal-compound parabolic concentrator, which preheats the saline or brackish water. Flat plate collectors integrated with solar stills are commercialized, but are not self-sustainable. For a self-sustainable active solar distillation system, electrical energy is required to operate a pump/motor, which overcomes the pressure drop in connecting insulated pipes. So, the integration of the semitransparent photovoltaic module is a novel idea.

Integration of photovoltaic thermal-compound parabolic concentrators (PVT-CPC) with a solar still concentrates global solar radiation into photovoltaic thermal collector, which heats the working fluid and additionally generates electricity (direct current). Recently, Singh and Tiwari [28] did a comparative performance analysis of solar stills (single and double slope solar still) integrated with PVT-CPC and performed an exergo, enviro-economic, and productivity analysis. They have concluded that active single slope solar still (SS-SS) gives 3% higher daily overall thermal efficiency and 2% higher daily productivity if the depth of water in the basin is 0.56 m. In their work, the working fluid in PVT-CPC collectors is brackish/saline water, which reduces the life of PVT-CPC collectors due to corrosion. To overcome this problem, in our proposed system, a helically coiled heat exchanger (copper) is placed inside the SS-SS. The heat exchanger is integrated to the thermal collectors [Type (a–c)] to make a closed loop, as shown in Fig. 1a–c.

Type (a) Partially covered photovoltaic thermal-compound parabolic concentrator (PVT-CPC) ($A_{rm}=0.25$ m^2, $A_{rc}=0.65$ m^2), proposed system

Type (b) Fully covered photovoltaic thermal-compound parabolic concentrator (PVT-CPC) ($A_{rm}=1$ m^2, $A_{rc}=0$ m^2)

Type (c) Flat plate collector-compound parabolic concentrator (FPC-CPC) ($A_{rm}=0$ m^2, $A_{rc}=1$ m^2)

In the proposed cases (I–III) the water mass (brackish water) and the working fluid (water) is used to obtain higher yield, which have not been considered earlier. The three cases (I–III), which are considered for the study are:

Table 1 Review of previous research work on passive and active single slope solar still, and double slope solar still

Serial no.	Design parameters	Description	Results	Authors	Remarks
Single slope passive solar still					
1.	Wind speed	Above critical mass, productivity increases with wind velocity	When $T_{gi} = T_{go}$, productivity increases with wind velocity	El-Sebaii [3]	–
2.	Water depth	Lower water mass in the basin	At 0.02 m, depth yield is 32.57% more than at 0.18 m	Tiwari and Tiwari [4]	–
3.	Phase change material	Paraffin wax as phase change material	67.18% higher than conventional solar still	Kabeel et al. [5]	–
4.	Mirror Boosters	Reflects solar radiation in excess	4–2 l/m^2/day at 890 W/m^2 solar intensity	Shanmugan et al. [6]	Mirror tracking arrangement is needed
5.	Nano-particles	Increases surface area for heat transfer	Increases productivity and efficiency	Gupta et al. [7]	–
6.	Pyramid solar still using absorbing plates	Carbon fiber-epoxy composites are used for absorbing plate	Increase of 109% of distillate water	Abdelal and Taamneh [8]	Performance is enhanced when graphene nano-plaletes in incorporated
Concentrating collectors integrated with single slope solar still					
7.	Parabolic trough photovoltaic thermal solar collector	At a given geometric concentration	Thermal efficiency increased by 58% and electrical efficiency 11%	Coventry [9]	–
8.	CPC-PVT-FPC	Concentrating sunlight with CPC	Thermal efficiency with MPP tracking is elevated	Proell et al. [10]	Losses in PV efficiency due to higher operating temperature
Single slope active solar still					
9.	Flat plate collectors with solar still	Wick and energy storage materials are used	Yield is 60% higher than conventional SS	Rajaseenivasan et al. [11]	Economic analysis shows production cost is lesser in FPC SS-SS
10.	PVT collectors with SS-SS	PVT collectors connected in series	4 PVT collectors; maximum yield $M_w = 50$ kg	Gaur and Tiwari [12]	–
11.	Concentrating evacuated tubular collectors with pyramid solar still	CPC assisted with tubular solar still	Productivity was 7770 ml/day	Arunkumar et al. [13]	–
Single slope solar still with cooling condensing cover					
12.	Nano-fluids and glass cover cooling	Micro-flakes with concentration (0.125–2%) and glass cooling	Yield is improved by 57.6% using graphite particles	Sharshir et al. [14]	Availability of cooling fluid is needed
13.	SS-SS with glass cover cooling	Film cooling parameters are implemented	Increases still efficiency by 6%	Bassam and Hijleh [15]	Cooling water is recycled
14.	Multi-wick solar still with cooling glass cover	Multi-wick with cooling glass cover	10% increase in distilled water is observed	Dhiman and Tiwari [16]	–
15.	Stepped solar still with cooling glass cover	Best film cooling parameters are optimized	Productivity increased by 8.2%	Samadony and Kabeel [17]	Availability of water is required
Passive double slope solar still					
16.	Nano-particles	Al_2O_3, TiO_2 and CuO–water based nano-fluids	Enhancement of annual yield by 19.10, 10.38 and 5.25%	Sahota et al. [18]	Problem of sedimentation, dispersion and clustering of NP_s
17.	Water flow over glass cover and hot water in lower basin	Collector is disconnected from the still during the off-sunshine hours	System gives 50% higher yield than ordinary double basin solar still	Tiwari [19]	Availability of water is required

Table 1 (continued)

Serial no.	Design parameters	Description	Results	Authors	Remarks
18.	Effect of water depth	Water depth from 1 to 5 cm	1 cm depth gives 17.38% higher production of water than single basin solar still	Elango and Murugavel [20]	–
19.	A basin type double slope multi-wick solar still	Black cotton wick compared to jute wick	Maximum yield as 4.5 l/m^2 day for black cotton	Pal et al. [21]	Availability of black cotton wick and jute wick
20.	Double slope solar still with mild steel plate with minimum mass of water and different wick material	Different wick materials such as cotton cloth, sponge sheet, coir mate, and waste cotton pieces	Still with rectangular aluminum fin covered with cotton cloth is more effective	Murugavel and Srithar [22]	Availability of different wicks
21.	Double slope solar still with rubber scrapers and double slope solar still (DS-SS) were designed	Small slope of a condensing cover of the still (3°)	Daily yield of 4.24 l/m^2 day with productivity of 63% compared to DS-SS	Sulttani et al. [23]	–
Active double slope solar still					
22.	Double slope solar still using flat plate solar collector and cooling glass cover	Function change in basin brine depth and glass cover thickness with glass cooling cover	Maximizes fresh water production (10.6 l/m^2 day)	Morad et al. [24]	Availability of water
23.	Effect of air velocity on the efficiency in a forced convective double slope solar still	Different average air velocities 2.5, 3.5, 5.5, and 6.9 m/s	Thermal efficiency increases up to 37.9% with 5.5 m/s wind speed and then decreases	Castillo-Tellez et al. [25]	Placing a transparent wind tunnel on solar still external cover
24.	A modified photovoltaic thermal DS-SS was designed	PVT collectors are arranged in parallel	Production rate was accelerated to 1.4 times than PVT-SS-SS	Singh et al. [26]	–
25.	Double slope solar still equipped with thermo-electric heating modules	Heating modules is used as water heater to increase the water temperature	Cost of distilled water for the day and night are 0.142 and 0.237 \$/L/m^2	Rahbar et al. [27]	–

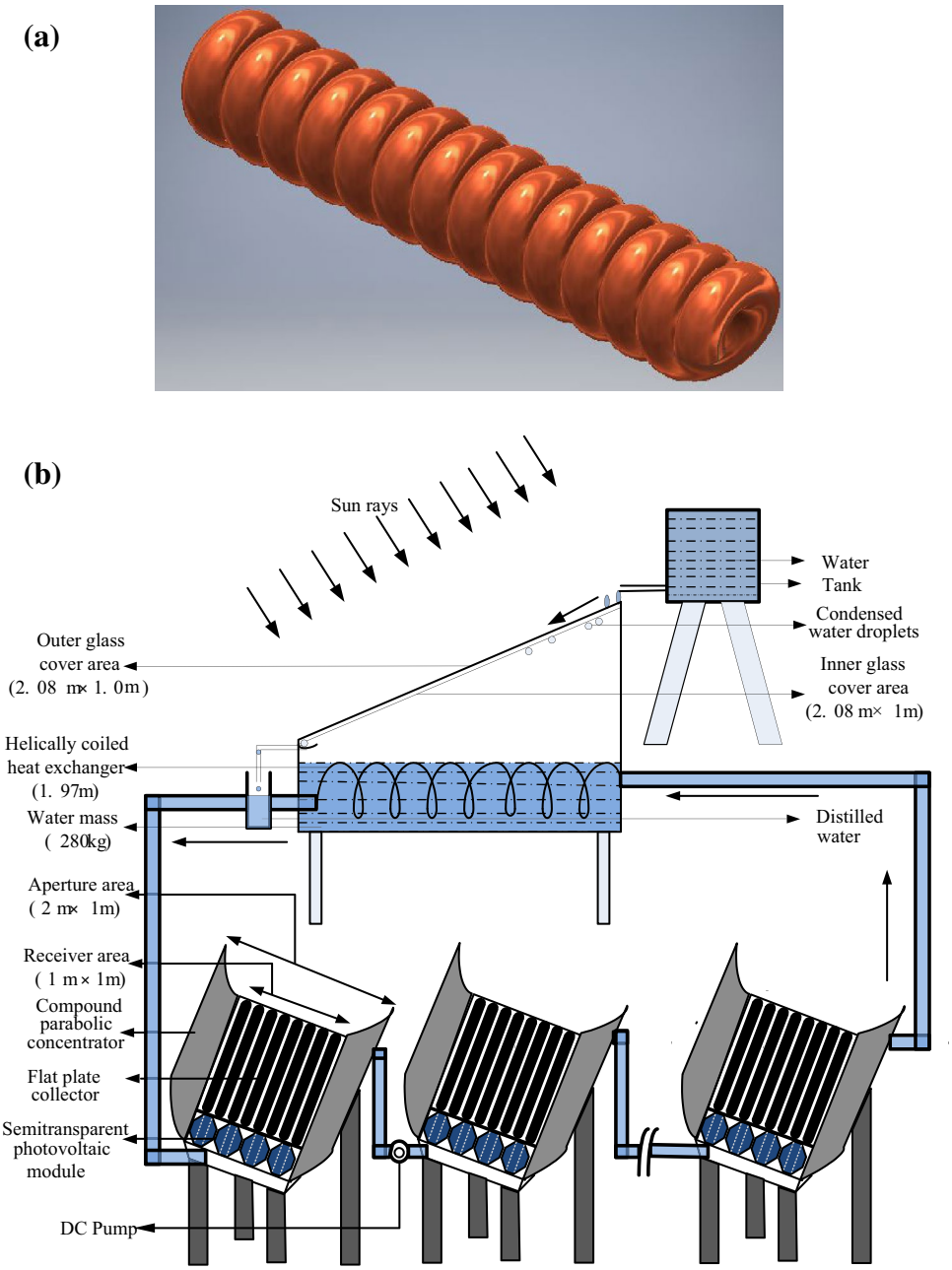

Fig. 1 **a** Helically coiled copper heat exchanger. **b** Schematic view of an active single slope solar still integrated with the help of a heat exchanger [case (I)]. **c** Schematic view of an active single slope solar still integrated with the help of a heat exchanger [case (II)]. **d** Schematic view of an active single slope solar still integrated with the help of a heat exchanger [case (III)]. **e** Schematic view of partially covered photovoltaic thermal flat plate collector (PVT-FPC) integrated with a single slope solar still

Case (I) Partially covered photovoltaic thermal-compound parabolic concentrator single slope solar still (PVT-CPC-SS-SS),

Case (II) Fully covered thermal-compound parabolic concentrator single slope solar still (PVT-CPC-SS-SS)

Case (III) Flat plate thermal-compound parabolic concentrator single slope solar still (FPC-CPC-SS-SS).

In addition, if cooling condensing cover over SS-SS with heat exchanger and thermal collector Type (a–c) are taken into account it will lead to higher distilled water as well as the life of solar thermal collectors will increase, which will make the system more viable economically.

As Singh and Tiwari [28] have not studied the effect of heat exchanger and cooling condensing cover of SS-SS. This paper deals with the energy and exergy analysis of the three active solar distillation units [cases (I–III)] for the optimum design. Moreover, energy matrices, production cost of distilled water and electricity, and co-generation efficiency have been analyzed and compared among three cases (I–III).

Fig. 1 (continued)

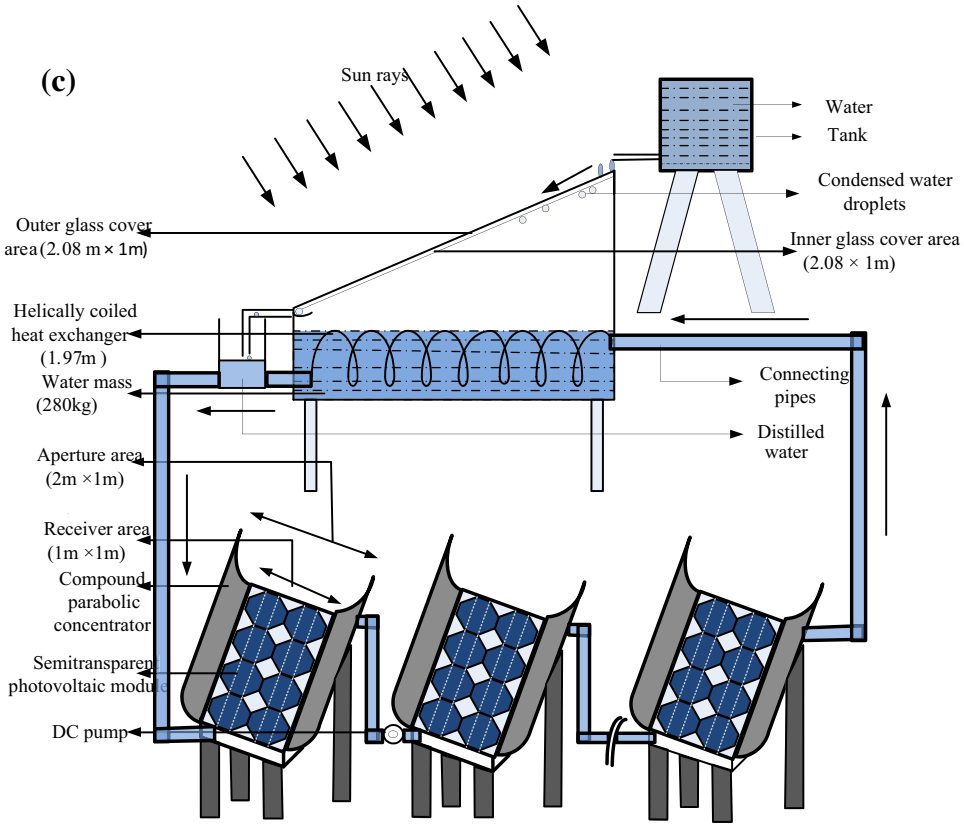

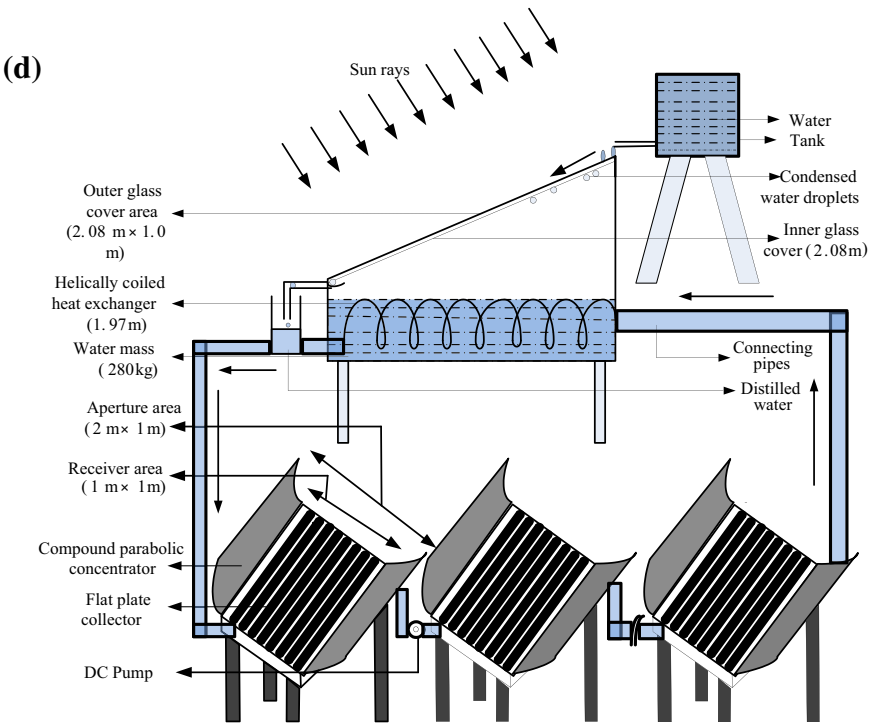

Fig. 1 (continued)

System description

The concentration ratio (c) of compound parabolic concentrator made up of (aluminum) for a given acceptance angle ($\theta_c = 30^\circ$) can be calculated from the following equation:

$$c = \frac{1}{\sin 2\theta_c}. \quad (1)$$

Rabl [29] derived an expression for aperture width, height, and arc length for the truncated compound parabolic concentrator (CPC). The side view of helically coiled copper heat exchanger (optimized numerically) with a length of 1865 mm having 14-helix with a pitch of 140 mm is shown in Fig. 1a. Figure 1b–d depicts three active solar still systems, i.e., PVT-CPC integrated with a SS-SS with the help of a heat exchanger. The CPC is inclined at 30° (latitude of New Delhi, India) toward south to receive the maximum annual global solar radiation (I_t), and concentrates global radiation falling on an aperture area towards the receiver area (I_b) for the three different configurations [Type (a–c)]. Thus, the fluid flowing beneath the photovoltaic thermal-compound parabolic collectors (PVT-CPC) Type (a–c) gets heated up at a faster rate compared to the photovoltaic thermal flat plate collector (PVT-FPC). Type (a) consists of a semitransparent PV module in the lower portion, and a flat plate collector at the upper portion of the receiver area and outlet from the semitransparent PV module is the inlet to the tube-in-flat plate collectors (Fig. 1b). This arrangement gives increased electrical efficiency because initially higher heat (generated by solar cells) is extracted by the fluid (water) flowing at the rear portion of PVT-CPC. Above-mentioned configurations [Type (a–c)] are arranged in series (to increase the water temperature), i.e., the outlet of first PVT-CPC is an inlet to the second and continues till Nth PVT - CPC to obtain maximum outlet fluid temperature and yield (Eqs. 8 and 21). The pressure drop in insulated connecting pipes is overcome by DC motor driven by the semitransparent PV modules.

The outlet of Nth PVT-CPC is connected to the basin of SS-SS with the help of helically coiled copper heat exchanger, and the outlet from SS-SS is connected to the first PVT-CPC. Thus, water circulates in a closed loop. The absorber plate (black dye-in-water solution) is placed in the SS-SS made up of fiber-reinforced plastic (FRP) having an effective basin area of 2 m^2. Cooling condensing cover has a thickness of 0.004 m inclined at an angle of 15° with the horizontal. Glass is recommended as a cooling condensing cover over plastic. The side walls are blackened so that maximum solar flux is absorbed inside the SS-SS. The whole system is sealed with the window putty and fixed on an iron stand. Table 2 gives detail specifications for three active SS-SS, cases (I–III), and thermal collectors Type (a–c).

Experimental validation

We have carried out experimental validation for a special case, i.e., SS-SS integrated with photovoltaic thermal flat plate collectors (PVT-FPCs) without heat exchanger. Experimental setup is shown in Fig. 1e. SS-SS made up of fiber-reinforced plastic has an effective area of 1 m^2, which is connected to three PVT-FPC through an insulated pipe. A DC motor has been used in a closed loop for forced mode of operation. The design parameters of the system are given in Table 3. Concentrating solar radiation ($I(t)$) into PVT-FPC, cooling of condensing cover and integration of helical coiled heat exchanger are excluded from the experimental unit. As the CPC is not included in the design the solar radiation falling on PVT-FPC is global radiation, which has lower intensity than beam radiation. In addition, cooling condensing cover is also removed, which reduces the temperature difference between glass and water in the basin, as a result the yield reduces. However, as the helical heat exchanger is

Table 2 Specifications of the hybrid active solar distillation systems, case (I–III)

Components	Specifications
Specifications for single slope solar still	
Length	2 m
Breadth	1 m
Inclination of glass cover	15°
Material of body	Fiber-reinforced plastic (FRP)
Material of stand	Galvanized iron
Condensing material	Glass
Orientation	South
Specifications of thermal collectors	
Type and number of collectors	Tube in plate type
Thickness of copper tubes	1 m
Tube diameter	0.0125 m
Angle of CPC with horizontal	30°
Thickness of CPC	0.004 m
Aperture area	2 m^2
Receiver area	1 m^2
Aperture area of module [Type (a), Type (b) and Type (c)]	0.5, 2 and 0 m^2
Aperture area of receiver [Type (a),Type (b) and Type (c)]	1.5, 0 and 2 m^2
Receiver area of module [Type (a), Type (b) and Type (c)]	0.25, 1 and 0 m^2
Receiver area of collector [Type (a), Type (b) and Type (c)]	0.75, 0 and 1 m^2
Specific heat capacity of fluid	4190 J/kg K
K_g	0.78 W/m^2 °C
L_g	0.003 m
K_i	0.166 W/m^2 °C
L_i	0.1 m
$U_{tc,p}$	2.67 W/m^2 °C
$U_{tc,a}$	19.34 W/m^2 °C
PF_1	0.12
PF_2	0.58
PF_c	0.98
h_{pf}	100 W/m^2 °C
h_i	2.8 W/m^2 °C
ρ	0.84
τ_g	0.95
α_c	0.7
β_c	0.8
$\propto_p$	0.6
F'	0.96
η_0	0.15

removed there is an increase in temperature of water (T_w) as there is direct transfer of hot water in the basin of solar still. The daily yield ($\dot{m}_{ew}$) obtained from PVT-FPC SS-SS is 3.85 kg for three PVT-FPC, which is lesser that the yield obtained from the proposed system [case (I)], i.e., 32.46 kg for the month of February.

Thermal model

The assumptions considered for the thermal modeling for different components of the active solar distillation systems to reduce complexity of the system are as follows:

Table 3 Design parameters of the photovoltaic thermal flat plate collector single slope solar still

Specifications of PVT-FPC active single slope solar still	
(a) Specifications of single slope solar still	
Length	1 m
Breadth	1 m
Inclination of glass cover	30°
Thickness of glass cover	0.004 m
(b) Specifications of photovoltaic module	
Area of single solar cell	0.007 m^2
Area of PV module	0.25 m^2
Efficiency of PV module	12%
Maximum power rating	40 W
$\propto_c$	0.9
η_o	0.15
β_o	0.0045/°C
β_c	0.89
(c) Specifications of flat plate collector	
τ_g	0.9
$\propto_p$	0.8
L_g	0.003 m
K_g	0.816 W/mK
L_i	0.1 m
K_i	0.166 W/mK
L_p	0.002 m
K_p	64 W/mK
C_f	4179 $\frac{J}{kg\,K}$
ρ	1000 kg/m^3
Area of collector A_c	1.75 m^2
h_i	5.8 W/m^2K
h_o	9.5 W/m^2K
Tube diameter	0.0125 m

1. The SS-SS and thermal collectors are in quasi-steady state.
2. Constant water mixing is preferred; thus, no stratification of water occurs in the basin of a SS-SS.
3. Ohmic losses in solar cells are neglected.
4. Heat capacity of the glass, solar cell, absorbing and insulating material used in the thermal collectors and SS-SS, and water flowing over the glass cover has been neglected.
5. The temperature gradients along the condensing cover thickness and water film have not been taken into account.
6. In SS-SS, film-type condensation occurs throughout the glass.

Energy balance equations for cooling condenser cover active SS-SS with helical heat exchanger [case (I)] are written as follow.

For water flowing over condensing cover:

$$\dot{m}_{f1} C_f \frac{dT_f}{dx} dx = [h_1(T_{go} - T_{wf}) - h_o(T_{wf} - T_a)]b dx. \quad (2)$$

For outer glass cover and inner glass cover:

$$h_{kg}(T_{gi} - T_{go})A_g = h_1(T_{go} - T_{wf})A_g \quad (3)$$

$$\alpha_g I(t)A_g + h_2(T_w - T_{gi})A_b = h_{kg}(T_{gi} - T_{go})A_g. \quad (4)$$

For water mass in the basin:

$$\dot{Q}_{u,N} + \alpha_w I(t)A_b + h_{bw}(T_b - T_w)A_b = M_w C_w \frac{dT_w}{dt} + h_2(T_w - T_{gi})A_b. \quad (5)$$

Useful energy gain from *N*th-PVT-CPC arranged in series combination

The energy balance equation for helical heat exchanger immersed in the basin of the SS-SS is given by

$$\dot{m}_f C_f \frac{dT_f}{dx} dx = -2\pi r_1 U(T_f - T_w). \quad (6)$$

Following boundary conditions is considered

$$T_w(x = 0) = T_{foN} \quad \text{and} \quad T_w(x = L) = T_{fi}.$$

Integrating Eq. 6 for the above mentioned boundary conditions, one can get

$$T_{fi} = T_{foN}\exp\left(\frac{-2\pi r_1 UL}{\dot{m}_f C_f}\right) + T_w\left(1 - \exp\left(\frac{-2\pi r_1 UL}{\dot{m}_f C_f}\right)\right), \quad (7)$$

where

$$U = \left[\frac{1}{h_w} + \left(\frac{r_1}{K_1}\right)\log\left(\frac{r_2}{r_1}\right) + \left(\frac{r_1}{r_2}\right)\frac{1}{h_w}\right]^{-1}.$$

Outlet fluid temperature (T_{foN}) for N thermal collector cases (a–c) can be obtained from the following equation:

$$T_{foN} = \left(\frac{I_b}{\dot{m}_f C_f}(AF_R(\alpha\tau)_1)\left(\frac{1 - K_K^N}{1 - K_K^N}\right)\right) + \left(\frac{T_a}{\dot{m}_f C_f}(AF_R U_L)_1\left(\frac{1 - K_K^N}{1 - K_K^N}\right)\right) + \left(T_{fi}K_K^N\right). \quad (8)$$

The rate of useful thermal energy obtained from thermal collectors can be calculated in Watt (W) from

$$\dot{Q}_{u,N} = \dot{m}_f C_f(T_{foN} - T_{fi}). \quad (9)$$

Substituting T_{foN} from Eq. 8 and rearranging Eq. 9 one can get

$$T_{\mathrm{fo}N} - T_{\mathrm{fi}} = \frac{I_{\mathrm{b}}\left(\frac{(AF_{\mathrm{R}}(\alpha\tau))_1}{\dot{m}_{\mathrm{f}}C_{\mathrm{f}}}\right)\frac{(1-K_{\mathrm{K}}^N)}{(1-K_{\mathrm{K}})}FR_1}{1-K_{\mathrm{K}}^N FR_2} + \frac{T_{\mathrm{a}}\left(\frac{(AF_{\mathrm{R}}U_{\mathrm{L}})_1}{\dot{m}_{\mathrm{f}}C_{\mathrm{f}}}\right)\frac{(1-K_{\mathrm{K}}^N)}{(1-K_{\mathrm{K}})}FR_1}{1-K_{\mathrm{K}}^N FR_2} - \frac{T_{\mathrm{w}}(1-K_{\mathrm{K}}^N)FR_1}{(1-K_{\mathrm{K}}^N FR_2)}. \tag{10}$$

Rate of useful thermal energy from Eq. 9 for case (i) can be expressed as

$$\dot{Q}_{\mathrm{u},N} = \frac{I_{\mathrm{b}}(AF_{\mathrm{R}}(\alpha\tau))_1(1-K_{\mathrm{K}}^N)FR_1}{(1-K_{\mathrm{K}})(1-K_{\mathrm{K}}^N FR_2)} + \frac{T_{\mathrm{a}}(1-K_{\mathrm{K}}^N)(\dot{m}_{\mathrm{f}}C_{\mathrm{f}})FR_1}{(1-K_{\mathrm{K}}^N FR_2)} - \frac{T_{\mathrm{w}}(1-K_{\mathrm{K}}^N)(\dot{m}_{\mathrm{f}}C_{\mathrm{f}})FR_1}{(1-K_{\mathrm{K}}^N FR_2)}, \tag{11}$$

where $(AF_{\mathrm{R}}(\alpha\tau))_1$, $(AF_{\mathrm{R}}U_{\mathrm{L}})_1$, FR_1, FR_2, and K_{K} are given in "Appendix".

For basin liner:

$$\alpha_{\mathrm{b}}I(t)A_{\mathrm{b}} = h_{\mathrm{bw}}(T_{\mathrm{b}} - T_{\mathrm{w}})A_{\mathrm{b}} + h_{\mathrm{ba}}(T_{\mathrm{b}} - T_{\mathrm{a}})A_{\mathrm{b}}. \tag{12}$$

Solving Eqs. (2–4) one can get

$$\frac{\mathrm{d}T_{\mathrm{wf}}}{\mathrm{d}x} + a_1 T_{\mathrm{wf}} = f(t)_1. \tag{13}$$

The solution of first-order differential Eq. 13 can be written as

$$T_{\mathrm{wf}} = \frac{\overline{f(t)_1}}{a_1}(1 - \exp(-a_1 x)) + T_{\mathrm{wfi}}\exp(-a_1 x). \tag{14}$$

Integrating Eq. 14 along the length of glass $x = l$

$$\overline{T_{\mathrm{wf}}} = \frac{\overline{f(t)_1}}{a_1}\left(1 - \frac{(1-\exp(-a_1 l))}{a_1 l}\right) + T_{\mathrm{wfi}}\frac{1-\exp(-a_1 l)}{-a_1 l}, \tag{15}$$

where T_{wfi} is the inlet water temperature flowing over the condensing cover, and $\overline{f(t)_1}$ is the average value between-length $l = 0$ to l where

$$f(t)_1 = \left(\frac{I(t)_2 + (UA)_{\mathrm{w,wf}}T_{\mathrm{w}}b + h_{\mathrm{o}}bT_{\mathrm{a}}}{\dot{m}_{\mathrm{f1}}C_{\mathrm{f}}}\right); \quad a_1 = \frac{(UA_{\mathrm{w,wf}}b) + (h_{\mathrm{o}}b)}{\dot{m}_{\mathrm{f1}}C_{\mathrm{f}}}.$$

Solving Eqs. 3 and 4 with the help of Eq. 15 and substituting T_{gi}, T_{b}, and $\dot{Q}_{\mathrm{u},N}$ in Eq. 5 one can get

$$T_{\mathrm{w}} = \frac{\overline{f(t)_2}}{a_2}(1 - \exp(-a_2\Delta t)) + T_{\mathrm{wo}}\exp(-a_2\Delta t), \tag{16}$$

where $f(t)_2 = \frac{(A_{\mathrm{b}}(T)+W(Y(Z+U1)+V)+X)}{M_{\mathrm{w}}C_{\mathrm{w}}}$and

$$a_2 = \frac{T_{\mathrm{w}}}{M_{\mathrm{w}}C_{\mathrm{w}}}\left((U_{\mathrm{bca}}A_{\mathrm{b}}) + \frac{h_2A_{\mathrm{b}}A_{\mathrm{g}}h_{\mathrm{kg}}(1-C_1)}{(h_{\mathrm{kg}}A_{\mathrm{g}}) + (h_2A_{\mathrm{b}})}\right)$$

$$T_{\mathrm{b}} = \frac{\alpha_{\mathrm{b}}\,I(t) + h_{\mathrm{bw}}T_{\mathrm{w}} + h_{\mathrm{wa}}T_{\mathrm{a}}}{h_{\mathrm{bw}} + h_{\mathrm{ba}}} \tag{17}$$

$$T_{\mathrm{go}} = T_{\mathrm{w}}\left[\frac{(UA)_{\mathrm{wgo}}}{h_1A_{\mathrm{g}} + (UA)_{\mathrm{wgo}}} + \frac{h_1A_{\mathrm{g}}}{h_1A_{\mathrm{g}} + (UA)_{\mathrm{wgo}}} \times \frac{(UA)_{\mathrm{w,wf}}}{(UA)_{\mathrm{w,wf}} + h_{\mathrm{o}}}\left(1 - \frac{1-\exp(-a_2 l)}{a_2 l}\right)\right] + \left(\frac{(It)_{\mathrm{A}}}{h_1A_{\mathrm{g}} + (UA)_{\mathrm{wgo}}} + \frac{h_1A_{\mathrm{g}}}{h_1A_{\mathrm{g}} + (UA)_{\mathrm{wgo}}}S\right) \tag{18}$$

$$T_{\mathrm{gi}} = \frac{\alpha_{\mathrm{g}}I(t)A_{\mathrm{g}}}{h_{\mathrm{kg}}A_{\mathrm{g}} + h_2A_{\mathrm{b}}} + T_{\mathrm{w}}\left[\frac{(h_2A_{\mathrm{b}}) + (h_{\mathrm{kg}}A_{\mathrm{g}}C_1)}{h_{\mathrm{kg}}A_{\mathrm{g}} + h_2A_{\mathrm{b}}}\right] + \left[\frac{h_{\mathrm{kg}}A_{\mathrm{g}}}{h_{\mathrm{kg}}A_{\mathrm{g}} + h_2A_{\mathrm{b}}}\left\{\frac{h_1A_{\mathrm{g}}}{h_1A_{\mathrm{g}} + (UA)_{\mathrm{wgo}}}S + \frac{(It)_A}{h_1A_{\mathrm{g}} + (UA)_{\mathrm{wgo}}}\right\}\right] \tag{19}$$

$$C_1 = \frac{(UA)_{\mathrm{wgo}}}{h_1A_{\mathrm{g}} + (UA)_{\mathrm{wgo}}} + \left(\frac{h_1A_{\mathrm{g}}}{h_1A_{\mathrm{g}} + (UA)_{\mathrm{wgo}}}\frac{(UA)_{\mathrm{w,wf}}}{(UA)_{\mathrm{w,wf}} + h_o}\left(1 - \frac{1-\exp(-a_2 l)}{a_2 l}\right)\right)$$

$$S = \frac{((It)_3 + h_{\mathrm{o}}T_{\mathrm{a}})}{(UA_{\mathrm{wwf}} + h_{\mathrm{o}})}\left(1 - \frac{1-\exp(-a_2 l)}{a_2 l}\right) + T_{\mathrm{wfi}}\left(\frac{1-\exp(-a_2 l)}{a_2 l}\right).$$

Unknown terms are expressed in "Appendix"

Electrical efficiency (η_{cN}) of semitransparent photovoltaic module at Nth collector for Type (a) and Type (b) can be obtained from the following equation:

$$\eta_{cN} = \frac{\eta_o\left[1-\beta_o\left[\frac{1}{U_{tcp}+U_{tca}}\left[(I_bZ_a)+T_a\left[U_{tca}+\frac{U_{tcp}U_{L1}}{U_{L2}+(F'h_{pf})}+(T_{a1}T_{a2})\right]+T_{fi}Z_b\right]-T_o\right]\right]}{1-\frac{\eta_o\beta_oI_b}{(U_{tcp}+U_{tca})}[Z_c]}. \tag{20}$$

Similarly, water temperature Eq. 16 for case (II) and case (III) can be obtained by substituting Type (b) and Type (c) design configurations in Eq. 8. The hourly yield, thermal energy ($E_{thermal}$) and thermal exergy ($Ex_{thermal}$) for the cases (I–III) can be obtained from

$$\dot{m}_{ew} = \frac{h_{ew}A_b(T_w - T_{gi})}{L} \times 3600 \tag{21}$$

and

$$Ex_{thermal} = h_{ew}A_b\left[(T_w - T_{gi}) - (T_a + 273)\times \ln\frac{T_w+273}{T_{gi}+273}\right], \tag{22}$$

where latent heat of vaporization $\left(\frac{kJ}{kg}\right)$ can be evaluated by Fernandez and Chargoy [30]

$$L = 3.1625\times10^6 + [1-(7.616\times10^{-4}\times T_w)] \quad \text{if } T_w > 70\ ^\circ\text{C}$$

$$L = 2.4935\times10^6[1-(9.4779\times T_w)+(1.3132\times10^{-7}\times T_w^2) - (4.7974\times10^{-3}\times T_w^3)] \quad \text{if } T_w < 70\ ^\circ\text{C}.$$

Thermal model for heat transfer

The temperature gradient in the fluid causes density variation in the humid air, which leads buoyant force and convective heat transfer in the solar still. Kumar and Tiwari [31] developed a thermal model based on regression method to determine convective (h_{cw}) and evaporative heat transfer coefficient (h_{ew}). They have considered the effects of solar still cavity, orientation of condensing cover (glass), operating temperature range during the thermal modeling, and assumed 100% relative humidity inside the solar still. This model can be used for the wider range of water temperature. The methodology carried out by Kumar and Tiwari [31] for the calculation of convective and evaporative heat transfer coefficient is as follows.

The rate of convective heat transfer from the water surface to the glass cover can be estimated by

$$\dot{q}_{cw} = h_{cw}(T_w - T_{gi})A_b, \tag{23a}$$

where h_{cw} can be calculated from

$$Nu = \frac{h_{cw}\times d_f}{k_f} = C(Gr.Pr)^n \tag{23b}$$

or

$$h_{cw} = \frac{C(Gr.Pr)^n k_f}{d_f}, \tag{23c}$$

where

$$Gr = \frac{g\beta'\rho^2(d_f)^3(\Delta T)'}{\mu^2}$$

$$Pr = \frac{\mu C_p}{k_f}$$

and

$$\Delta T = (T_w - T_{gi}) + \left[\frac{(P_w - P_{gi})(T_w+273)}{(268.9\times10^3)-P_w}\right].$$

From Eq. (23c) it is observed that 'h_{cw}' depends upon 'C' and 'n'. It was observed from different values of 'C' and 'n' for a particular range of Grashof number given by authors that the percentage deviation between experimental and theoretical is within reasonable percentage of accuracy for indoor simulated conditions; however, for outdoor conditions the deviation increases significantly. Thats why, Kumar and Tiwari [31] have modified the values of 'C' and 'n' for outdoor conditions.

The distillate output from an evaporative area (A_b) during time 't' can be expressed as

$$\dot{m}_{ew} = \frac{\dot{q}_{ew}\times t}{L}, \tag{23d}$$

where

$$\dot{q}_{ew} = A_b h_{ew}(T_w - T_{gi}) \tag{23e}$$

and

$$h_{ew} = 16\times10^{-3}\times h_{cw}\times\frac{(P_w - P_{gi})}{(T_w - T_{gi})}. \tag{23f}$$

Substituting, h_{cw} from Eq. (23c) in Eq. (23f)

$$h_{ew} = 0.0162\times C(Gr.Pr)^n\times\frac{k_f}{d_f}\frac{(P_w - P_{gi})}{(T_w - T_{gi})}. \tag{23g}$$

Further, substituting Eq. (23g) in Eq. (23e)

$$\dot{q}_{ew} = A_b \times 0.0165 \times C(Gr.Pr)^n \times \frac{k_f}{d_f} \times (P_w - P_{gi}) \quad (23h)$$

Substituting Eq. (23h) in Eq. (23d), we get

$$\dot{m}_{ew} = K_1 \times C(Gr.Pr)^n$$

$$\frac{\dot{m}_{ew}}{K_1} = C(Gr.Pr)^n, \quad (23i)$$

where

$$K_1 = \frac{0.0162}{L} \times \frac{k_f}{d_f} \times A_b \times t \times (P_w - P_{gi}).$$

Taking 'natural log' on both the sides of Eq. (23i) and comparing with $y = mx + C_o$, we get

$$\ln\left(\frac{\dot{m}_{ew}}{K_1}\right) = \ln C + n \ln(Gr.Pr),$$

where

$$y = \ln\left(\frac{\dot{m}_{ew}}{K_1}\right)$$

$$C_o = \ln C$$

$$x = \ln(Gr.Pr)$$

$$m = n,$$

$$\text{where } m = \frac{N\left(\sum_{i=1}^{N} x_i y_i\right) - \left(\sum_{i=1}^{N} x_i\right)\left(\sum_{i=1}^{N} y_i\right)}{N\left(\sum_{i=1}^{N} x_i^2\right) - \left(\sum_{i=1}^{N} x_i\right)^2}$$

$$C_o = \frac{\left(\sum_{i=1}^{N} y_i\right)\left(\sum_{i=1}^{N} x_i^2\right) - \left(\sum_{i=1}^{N} x_i\right)\left(\sum_{i=1}^{N} x_i y_i\right)}{N\left(\sum_{i=1}^{N} x_i^2\right) - \left(\sum_{i=1}^{N} x_i\right)^2}.$$

After calculating 'm' and 'C_o'

$$C = \exp(C_o)$$

and, $n = m$

Thus, convective and evaporative heat transfer coefficients can be calculated with the help of these constants (C, n) by substituting in Eq. (23c) and (23g).

The values of 'C', 'n', and Grahof number on the experimental day (20/2/2018) at 8 cm of water depth in the proposed hybrid active solar still are 2.79, 0.16, and 2.8×10^{-7} [31]. With these values, the convective (h_{cw}) and evaporative heat transfer (h_{ew}) are 2.5 W/m^2 and 35 W/m^2.

Regression analysis

To find the relation between experimental value (Table 4) and theoretical value (Table 4) of yield, correlation coefficient (r) and percentage deviation (e) are calculated where

$$r = \frac{N\sum_{i=1}^{N} X_i Y_i - \left(\sum_{i=1}^{N} X_i \sum_{i=1}^{N} Y_i\right)}{\sqrt{N\sum_{i=1}^{N} X_i^2 - \left(\sum_{i=1}^{N} X_i\right)^2}\sqrt{N\sum_{i=1}^{N} Y_i^2 - \left(\sum_{i=1}^{N} Y_i\right)^2}}$$

$$e = \sqrt{\frac{\sum_{i=1}^{N}\left(\frac{X_i - Y_i}{X_i}\right)^2}{N}} \times 100.$$

The coefficient of correlation and percentage deviation of PVT-FPC SS-SS is 0.99 and 4.86% for the month of February' 2018.

Performance parameters

Performance analysis of three active solar distillation system cases (I–III) have been evaluated on the bases of the first and the second laws of thermodynamics; following Jafarkazemi and Ahmadifard [32], Nag [33].

1. The overall thermal energy and exergy analysis

$$\dot{E}_{\text{daily, overall thermal}} = \sum_{t=1}^{24}[\dot{m}_{ew} L] + \frac{\sum_{t=1}^{10}[[NA_{am} I(t)_b(\alpha\tau_g\eta_{cN}\rho)] - \dot{P}_u]}{0.38} \quad (24)$$

$$\dot{E}x_{\text{daily, overall thermal}} = \sum_{t=1}^{24} h_{ew} A_b \left[(T_w - T_{gi}) - (T_a + 273) \times \ln\frac{T_w + 273}{T_{gi} + 273}\right] + \sum_{t=1}^{10}[[NA_{am} I(t)_b(\alpha\tau_g\eta_{cN}\rho)] - \dot{P}_u] \quad (25)$$

Collector exergy

$$= \sum_{t=1}^{10}(\dot{m}_f C_f)\left[\left(T_{foN} - T_{fi}\right) - \left((T_a + 273) \times \ln\frac{T_{foN} + 273}{T_{fi} + 273}\right)\right], \quad (26)$$

where T_{foN}, T_{fi}, and $\dot{P}_u$ represent the outlet fluid temperature at Nth PVT - CPC, inlet fluid temperature for the first PVT-CPC collector, and power consumed by the DC motor hourly. Thus, the daily thermal energy, the overall thermal energy, the overall thermal exergy, and

Table 4 Hourly variations of various parameters of the hybrid active solar still for 0.08 m water depth on 20th February, 2018: (a) experimental value and (b) theoretical value

Time	$I(t)_C\left(\frac{W}{m^2}\right)$	$I(t)_S\left(\frac{W}{m^2}\right)$	T_a (°C)	V_a (°C)	V_L (*V*)	I_L (*A*)	V_{OC} (*V*)	I_{SC} (*A*)	T_w (°C)	T_{gi} (°C)	T_b (°C)	$\dot{m}_{ew}\left(\frac{kg}{h}\right)$
(a) Experimental value												
08:00	70	70	12	1.2	0	0	0	0	14.58	13.34	14.72	0.0043
09:00	130	130	12	2	13.4	2.2	20.9	2.4	18.37	14.55	18.61	0.0091
10:00	330	330	16.5	1.05	14.3	2.7	20.2	4.2	29.96	23.74	30.60	0.0252
11:00	430	430	20	0.25	14.7	2.5	19.5	5.9	43.03	35.94	43.80	0.0609
12:00	470	470	23.5	0.5	16.9	3.3	19	7.6	53.99	45.89	54.78	0.143
13:00	510	510	24.5	1.75	16.5	2.8	19.2	7.5	61.29	50.58	62.11	0.3393
14:00	490	490	25.5	1.25	16.6	2.7	18.5	7.2	65.95	57.60	66.68	0.3951
15:00	450	450	27	1	15.6	2.6	18.3	5.2	68.26	61.29	68.89	0.4038
16:00	350	350	26	0.55	13.5	2.5	17.6	4.3	66.33	60.83	66.73	0.3456
17:00	210	210	25.5	0.9	13.1	2.3	16.2	3.5	59.30	53.40	59.43	0.3199
18:00	70	70	23.5	0.45	0	0	0	0	55.87	49.70	55.52	0.2396
19:00	50	50	20.5	0.55	0	0	0	0	52.45	45.48	52.11	0.2298
20:00	0	0	18.5	0.45	0	0	0	0	49.31	42.25	48.9	0.1996
21:00	0	0	17.1	0.55	0	0	0	0	46.31	38.76	46.0	0.1821
22:00	0	0	15.9	0.05	0	0	0	0	43.86	37.52	43.57	0.1324
23:00	0	0	14.3	0.45	0	0	0	0	41.27	33.48	40.98	0.1391
24:00	0	0	14.3	0.55	0	0	0	0	38.88	31.21	38.62	0.1236
01:00	0	0	13.5	1.05	0	0	0	0	36.46	27.80	36.21	0.1226
02:00	0	0	13	1.05	0	0	0	0	34.26	25.91	34.035	0.1055
03:00	0	0	13	1.05	0	0	0	0	32.30	24.40	32.09	0.0884
04:00	0	0	12.5	1.05	0	0	0	0	30.51	22.86	30.32	0.0764
05:00	0	0	12.5	1.05	0	0	0	0	28.91	21.72	28.73	0.0648
06:00	0	0	11.5	1.05	0	0	0	0	27.38	20.22	27.21	0.0585
07:00	0	0	11.5	1.05	0	0	0	0	26.00	19.31	25.85	0.0502
(b) Theoretical value												
08:00	70	70	12	1.2	0	0	0	0	14.67	13.38	14.85	0.0045
09:00	130	130	12	2	13.4	2.2	20.9	2.4	18.60	14.64	18.92	0.0096
10:00	330	330	16.5	1.05	14.3	2.7	20.2	4.2	30.54	24.04	31.37	0.0269
11:00	430	430	20	0.25	14.7	2.5	19.5	5.9	43.97	36.64	44.99	0.0655
12:00	470	470	23.5	0.5	16.9	3.3	19	7.6	55.21	46.95	56.26	0.154
13:00	510	510	24.5	1.75	16.5	2.8	19.2	7.5	62.67	51.90	63.78	0.3643
14:00	490	490	25.5	1.25	16.6	2.7	18.5	7.2	67.42	59.11	68.42	0.4217
15:00	450	450	27	1	15.6	2.6	18.3	5.2	69.74	62.85	70.62	0.4295
16:00	350	350	26	0.55	13.5	2.5	17.6	4.3	67.71	62.29	68.30	0.3659
17:00	210	210	25.5	0.9	13.1	2.3	16.2	3.5	60.42	54.58	60.68	0.3384
18:00	70	70	23.5	0.45	0	0	0	0	56.87	50.73	56.52	0.2522
19:00	50	50	20.5	0.55	0	0	0	0	53.34	46.38	52.99	0.2412
20:00	0	0	18.5	0.45	0	0	0	0	50.10	43.04	49.76	0.2088
21:00	0	0	17.1	0.55	0	0	0	0	47.01	39.44	46.69	0.1901
22:00	0	0	15.9	0.05	0	0	0	0	44.50	38.14	44.19	0.1378
23:00	0	0	14.3	0.45	0	0	0	0	41.84	34.01	41.54	0.1446
24:00	0	0	14.3	0.55	0	0	0	0	39.39	31.66	39.12	0.1284
01:00	0	0	13.5	1.05	0	0	0	0	36.91	28.17	36.66	0.1272
02:00	0	0	13	1.05	0	0	0	0	34.65	26.23	34.42	0.1092
03:00	0	0	13	1.05	0	0	0	0	32.65	24.67	32.45	0.0913
04:00	0	0	12.5	1.05	0	0	0	0	30.83	23.09	30.63	0.0788
05:00	0	0	12.5	1.05	0	0	0	0	29.19	21.92	29.01	0.0668

Table 4 (continued)

Time	$I(t)_C\left(\frac{W}{m^2}\right)$	$I(t)_S\left(\frac{W}{m^2}\right)$	T_a (°C)	V_a (°C)	V_L (*V*)	I_L (*A*)	V_{OC} (*V*)	I_{SC} (*A*)	T_w (°C)	T_{gi} (°C)	T_b (°C)	$\dot{m}_{ew}\left(\frac{kg}{h}\right)$
06:00	0	0	11.5	1.05	0	0	0	0	27.63	20.40	27.46	0.0602
07:00	0	0	11.5	1.05	0	0	0	0	26.23	19.47	26.08	0.0516

Table 5 Optimized parameters for Type (a–c) for the months of June and January

S. no.	Cases	Mass flow rate (CC) (kg/s)	Heat exchanger (m)	Mass of water (kg)	No. of collectors	Mass flow rate (kg/s) (collector)
1.	Type (a)					
	June	0.025	1.97	280	6	0.04
	January	0.025		280	7	0.04
2.	Type (b)					
	June	0.025	1.97	280	8	0.04
	January	0.025		250	10	0.04
3.	Type (c)					
	June	0.025	1.97	280	5	0.04
	January	0.025		280	6	0.04

Table 6 Daily energy and exergy for the months of January and June for the three cases (I–III)

S. no.	Parameters	Case (I)		Case (II)		Case (III)	
		June (kWh)	January (kWh)	June (kWh)	January (kWh)	June (kWh)	January (kWh)
1.	Thermal energy	27.08	24.08	16.86	11.36	28.59	26.56
2.	Overall thermal energy	29.75	28.81	33.64	39.84	28.06	26.07
3.	Overall exergy	2.82	3.87	7.00	11.44	1.86	2.59
4.	Collector exergy	1.62	3.21	–	–	1.87	3.70

Table 7 Energy payback time, energy production factor, and life cycle conversion efficiency on the basis of energy and exergy for the three cases (I–III)

S. no.	Parameters	Case (I)	Case (II)	Case (III)
1.	Total embodied energy (kWh)	9556.34	18,209.50	7023.50
2.	Annual yield (kg)	8126.48	5451.28	8743.48
3.	Annual overall thermal energy available from SS-SS (kWh)	6347.30	7776.48	6123.25
4.	Annual overall thermal exergy available from SS-SS (kWh)	591.22	1715.89	345.86
5.	Energy payback time based on energy (years)	1.50–2	2.34	1.14-2
6.	Energy payback time based on exergy (years)	17	10.61	20
7.	Energy production factor based on energy	0.66	0.42	0.87
8.	Energy production factor based on exergy	0.06	0.09	0.04
9.	Life	50	50	50
10.	Solar radiation for life time (kWh)	9,77,464	12,00,753	8,47,541
11.	Life cycle conversion efficiency based on energy	0.31	0.30	0.35
12.	Life cycle conversion efficiency based on exergy	0.022	0.06	0.002

the collector exergy have been evaluated and are represented in Table 6. Here, it should be noted that after sunshine hours, yield ($\dot{m}_{ew}$) is continuously obtained from the active solar stills [case (I–III)] because water mass in the basin acts as a thermal storage.

2. Economic analysis

The evaluation of energy matrices is an important tool for the renewable energy technologies (RES) to be successful. Energy matrices include the study of (1) energy payback time (EPBT), (2) energy production factor (EPF), and (3) life cycle conversion efficiency (LCCE) of the system, Tiwari and Mishra [34]. Table 7

Table 8 Embodied energy of the three hybrid distillation systems case (I–III)

S. no.	Name of components	Embodied energy (kWh)		
		Case (I)	Case (II)	Case (III)
1.	Single slope solar still	1737.79	1737.7	1737.7
2.	Heat exchanger	350.5	350.5	350.5
3.	Compound parabolic concentrator collector	5733	7371	4914
4.	Photovoltaic module (glass to glass)	1715	8731.8	0
5.	Others	20.00	20.00	20.00
Total embodied energy (kWh)		9556.34	18,209.50	7023.50

Table 9 Capital investment for the three hybrid solar distillation systems [case (I–III)]

S. no.	Cost of components	Cost of system (₹)		
		Case (I)	Case (II)	Case (III)
1.	Single slope solar still	23,143	23,143	23,143
2.	Photovoltaic thermal-compound parabolic concentrator @10,500	73,500	0	0
3.	Photovoltaic module-compound parabolic concentrator @17,750	0	1,59,750	0
4.	Flat plate collector-compound parabolic concentrator @9250	0	0	55,500
5.	Heat exchanger	5100	5100	5100
6.	Motor/pump	1000	1000	1000
7.	Fabrication	6000	6000	6000
8.	Total capital investment	1,08,743	1,94,993	90,743

Table 10 Uniform end-of-year annual cost for the three hybrid solar distillation systems case (I–III)

S. no.	n (years)	i (%)	P_s (Rs)	M @ 10%	S_s (Rs)	$F_{CR,i,n}$	$S_{SR,i,n}$	UAC (₹)
Case (I)								
1.	50	2	1,08,743	10,874	29,251	0.031	0.01	3386
2.	50	5	1,08,743	10,874	1,24,699	0.054	0.004	5960
3.	50	10	1,08,743	10,874	12,76,543	0.1	0.00085	10,876
Case (II)								
4.	50	2	1,94,993	19,499	52,484	0.031	0.01	6071
5.	50	5	1,94,993	19,499	2,23,606	0.054	0.004	10,688
6.	50	10	1,94,993	19,499	22,89,039	0.1	0.00085	19,503
Case (III)								
7.	50	2	90,743	9074	24,424	0.031	0.01	2825.6
8.	50	5	90,743	9074	1,04,058	0.054	0.004	4973.8
9.	50	10	90,743	9074	10,65,239	0.1	0.00085	9076.2

represents energy matrices of the cases (I–III) based on energy and exergy.

3. Production cost of distilled water (₹/kg) and electricity generation (₹/kWh)

Initially, total embodied energy (kWh) (Table 8) for the three hybrid solar distillation systems cases (I–III) is calculated. Then, the capital investment for the three hybrid solar distillation systems is calculated from Eq. 27 (Table 9). In the cost analysis, replacement period of pump/motor is considered to be 10, 20, and 30 years, respectively. Following Tiwari and Mishra [34], a mathematical expression for capital recovery factor ($F_{CR,i,n}$), sinking fund factor ($S_{CR,i,n}$), and uniform end-of-year annual cost (UAC) is calculated in Table 10. Following Kumar and Tiwari [35], production cost of distilled water (C_{wp}) (₹/kg) and electricity generation (C_e)(₹/kWh) is calculated (Table 11) from Eq. 27

$$P = P_{SS\_SS} + P_{HE} + P_{CPC\_collector} + P_{PVM} + P_{fabrication}$$

$$\begin{aligned} &\mathrm{UAC} = (P_s \times F_{CR,in}) + (M_s \times F_{CR,in}) - (S_S \times F_{SR,in});\\ &C_{wp} = \frac{\mathrm{UAC} - R_e}{M_w}; \quad C_e = \frac{\mathrm{UAC} - R_w}{E_e}. \end{aligned} \tag{27}$$

Table 11 Production cost of distilled water obtained from the three cases (I–III)

S. no.	i (%)	UAC (Rs)	M_w (kg)	E_e (kWh)	$(SP)_w$ (₹/kg)	$(SP)_e$ (₹/kWh)	R_w (₹)	Re (₹)	UAC-R_e (₹)	UAC-R_w (₹)	C_{wp} (₹/kg)	C_e (₹/kWh)
Case (I)												
1.	2	3386	8126	490	5	5	40,632	2450	936	0	0.11	0
2.	5	5960	8126	490	5	5	40,632	2450	3510	0	0.43	0
3.	10	10,876	8126	490	5	5	40,632	2450	8426	0	1.03	0
Case (II)												
4.	2	6071	5451	1582	5	5	27,255	7910	0	0	0	0
5.	5	10,688	5451	1258	5	5	27,255	7910	2778	0	0.50	0
6	10	19,503	5451	1582	5	5	27,255	7910	11,593	0	2.12	0
Case (III)												
7	2	2825.6	8743	0	5	5	43,717	0	2825.6	0	0.32	0
8	5	4973.8	8743	0	5	5	43,717	0	4973.8	0	0.56	0
9	10	9076.2	8743	0	5	5	43,717	0	9076.2	0	1.03	0

Table 12 Co-generation efficiency for the hybrid solar distillation system [case (I–II)]

S. no.	Cases	Co-generation efficiency (%)
1.	Case (I)	44
2.	Case (II)	24

Here, R_w, R_e, and UAC represent the revenue earned from water and electricity, and uniform end-of-year annual cost obtained from the three cases (I–III). If UAC $- R_e$ or UAC $- R_w$ gives negative term, it is considered to be zero, which means the revenue obtained from the other source is capable to overcome the total cost of the system.

4. Co-generationefficiency

Co-generation is the simultaneous generation of electricity (kWh) and thermal energy (kWh). The production of electricity in conventional power plant releases heat (thermal energy), which is discarded as waste, whereas in co-generation this thermal energy is utilized for heating. From case (I) and case (II), electricity (power) is generated by glass-to-glass photovoltaic module and thermal energy (yield) simultaneously, due to solar energy (Table 12). Here, the electrical energy obtained is the net difference between electricity generated and consumed by the DC motor. Following Onovwiona and Ugursal [36], co-generation efficiency of the case (I) and (III) can be expressed as follows:

$$\eta_{cog} = \frac{\text{Electrical energy} + \text{thermal energy}}{\text{Solar radiation input to the system}}. \quad (28)$$

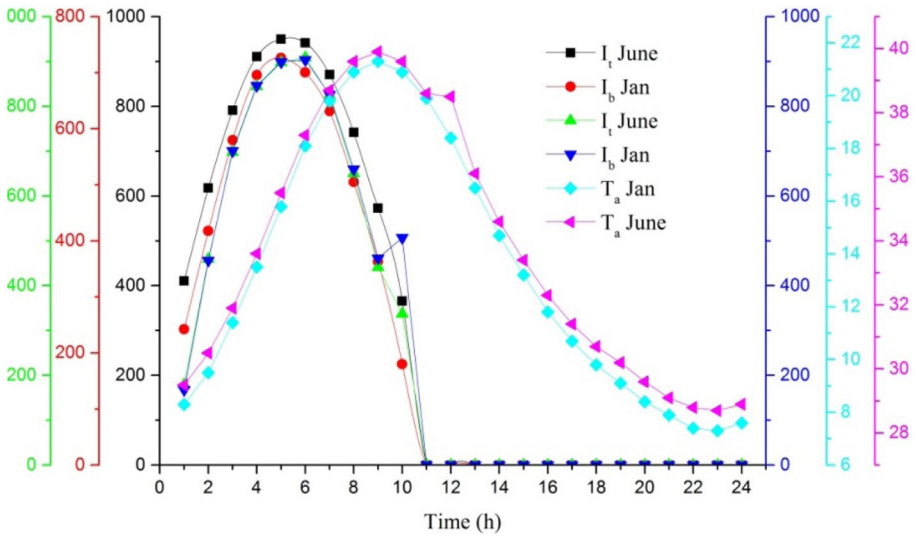

Fig. 2 Hourly variation of global, beam solar radiation, and ambient temperature for the months of January and June, respectively

Methodology

The following methodology is carried out for the study of three hybrid distillation systems:

Step (i) Initially following Lui and Jordan formulae [37], beam radiation (I_b) (Online resource 1) for PVT-CPC kept an angle of 30° from the horizontal and global radiation ($I(t)$) (Online resource 1) for the condensing cover inclined at 15° on SS-SS facing southwards is calculated for the months of January and June (Fig. 2). Further annual calculations of I_b (Online resource 1) and $I(t)$ (Online resource 1) is carried out simultaneously by the summation of solar intensity for the different months, which is done by multiplying daily solar radiation with number of clear days, hazy days, hazy and cloudy days, and cloudy days for a given month.

Step (ii) Optimizing the parameters for maximizing outlet fluid temperature (T_{foN}) (Eq. 8), module efficiency (η_m) (Eq. 20) and useful gain ($\dot{Q}_{u,N}$) (Eq. 11) have been carried out for three Type (a–c) on hourly, daily, and monthly bases. On the basis of numerical computation, optimized parameters are given in Table 5.

Step (iii) Further, water temperature (T_w), basin temperature (T_b), inner glass temperature (T_{gi}), and hourly yield ($\dot{m}_{ew}$) are calculated hourly and daily using Eqs. 16, 17, 19, and 21. Then, performance parameters, energy matrices, embodied energy (kWh), production cost of distilled water (C_{wp}) and electricity (C_e), and co-generation efficiency are obtained from Eqs. 24–28.

Thereafter, cases (I–III) are compared on the bases of computed numerical values.

Numerical computation

Case (A) Optimization of the number of thermal collectors, length of heat exchanger, mass flow rate in PVT-CPC collector loop, and above condensing cover

Optimization of the three active distillation system parameters assists for the maximum yield ($\dot{m}_{ew}$), exergy ($Ex_{thermal}$), and lowers energy back time (EPBT) and production cost of distilled water and electricity (C_{wp} and C_e). Figure 3a–c shows that at the lower mass flow rate ($\dot{m}_f$) higher outlet fluid temperature (T_{foN}) (Eq. 8) is obtained for the month of June for all three Type (a–c). At higher mass flow rate, the curves for the months of January and June intersect each other at the high number of thermal collectors (N). This is because thermal losses are maximum at higher operating temperature for the month of June. That's why, after four thermal collectors [case (I)] the outlet fluid temperature (T_{foN}) for the month of January dominates. A similar effect is observed by Singh and Tiwari [28]. Thus, the optimization of mass flow rate for thermal collectors [Type (a–c)]

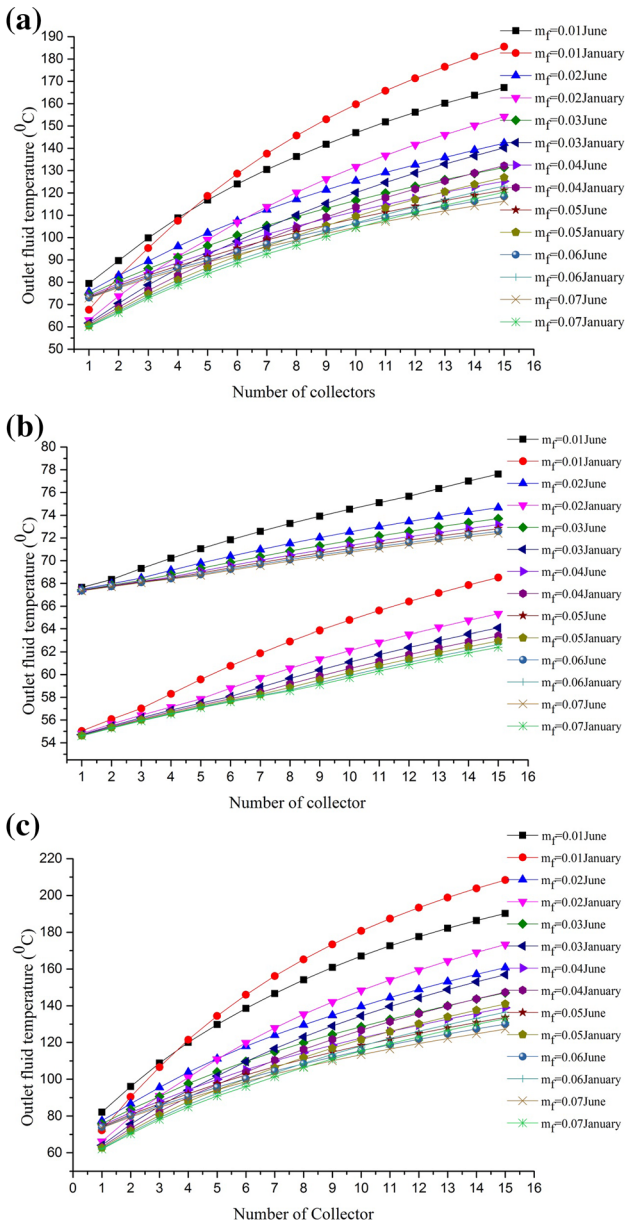

Fig. 3 **a** Variation of outlet fluid temperature with the number of collectors at a given mass flow rate for case (I) for the months of January and June, respectively. **b** Variation of outlet fluid temperature with the number of collectors at a given mass flow rate for case (II) for the months of January and June, respectively. **c** Variation of outlet fluid temperature with the number of collectors at a given mass flow rate for case (III) for the months of January and June, respectively

and water flowing above condensing cover and number of thermal collectors for three Type (a–c) is carried out and represented in Table 5. Case (II) has lesser thermal losses as outlet fluid temperature (T_{foN}) reaches the maximum of 75 and 66 °C for 0.01 kg/s mass flow rate in the months of June and January, respectively. Similarly, for the case (III)

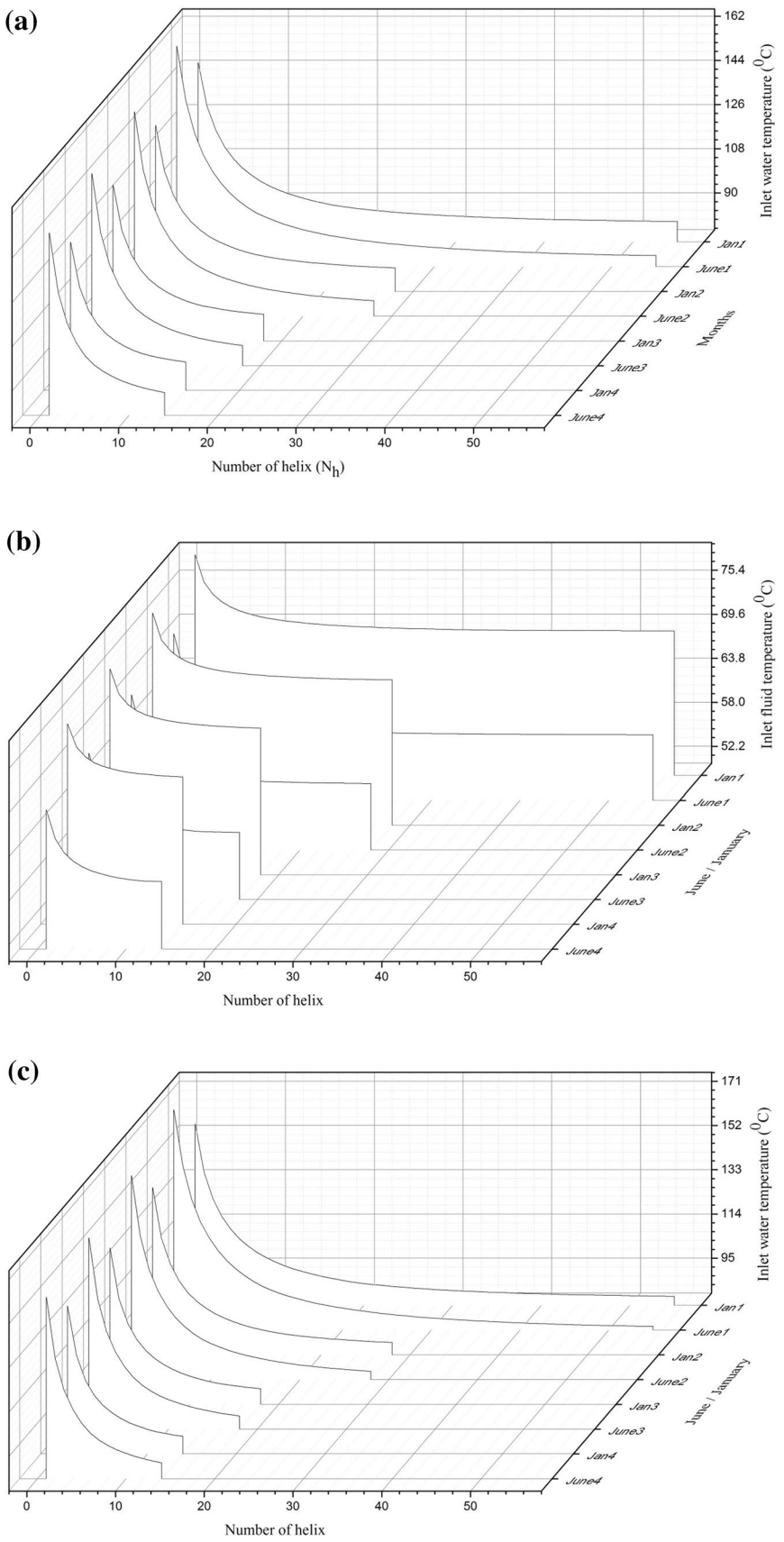

Fig. 4 **a** Variation of inlet fluid temperature with the number of helix of heat exchanger for case (I) for the months of January and June, respectively. **b** Variation of inlet fluid temperature with the number of helix of heat exchanger for case (II) for the months of January and June, respectively. **c** Variation of inlet fluid temperature with the number of helix of heat exchanger for case (III) for the months of January and June, respectively

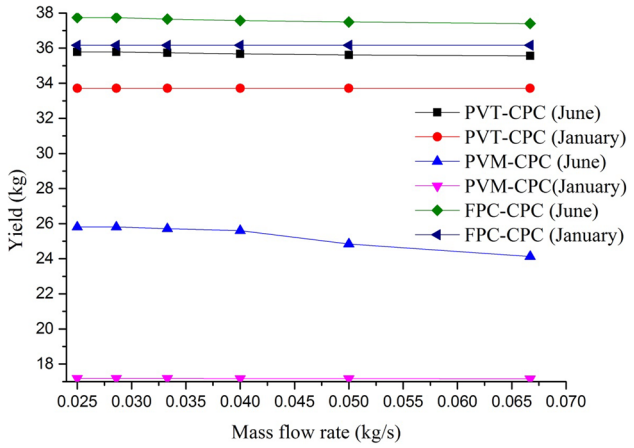

Fig. 5 Variation of yield with the mass flow rate flowing over condensing cover for three cases (I–III) for the months of January and June, respectively

after three thermal collectors the outlet fluid temperature (T_{foN}) for the month of January dominates compared to the month of June at a mass flow rate of 0.01 kg/s. Now, the maximum thermal heat is transferred to the brackish water mass in the basin by the optimization for number of helix (14) and pitch (0.05 m) of heat exchanger (Fig. 4a–c) for the months of June and January, respectively. For maximizing the overall heat transfer coefficient (U) from the heat exchanger of length (L), different pitches ranging from (0.0125 to 0.05 m) and helix (55, 35, 28 and 14) are considered for the minimum inlet fluid temperature (T_{fi}). In Fig. 4a, [case (I)] the minimum inlet water temperature is obtained for the months of June and January as 79 and 86 °C, respectively, for the configuration having 14 helix of 0.05 m pitch. Minimum inlet water temperature (T_{fi}) in the month of June clearly signifies that more heat transfer occurs from the fluid inside the heat exchanger (water) to the brackish water in the basin compared to January. Other configuration of the heat exchanger also follows the same behavior. Similarly, for the cases (II) and (III), the minimum inlet water temperature (T_{fi}) is 69, 58 °C and 87, 86 °C (Fig. 4b, c) for the configuration of 14-helix and 0.05 m pitch. So, this configuration is optimized for maximum overall heat transfer, among others for the months of June and January, respectively, for three configurations cases (I–III). Water flowing above condensing cover has a significant role on the overall performance of the active solar distillation systems cases (i–iii). A uniform water mass flowing over the condensing cover ($\dot{m}_{fl}$) remarkably increases the yield (distilled water) (Eq. 21) obtained from the solar still, as shown in Fig. 5. The reason behind it is that as the temperature difference between brackish water in the basin (T_w) and inner glass (T_{gi}) increases, the yield increases ($\dot{m}_{ew}$) (Eq. 21). The mass flow rate of water flowing over condensing cover is reduced from 0.065 to 0.025 kg/s simultaneously with the decrease in temperature to maximize yield (energy) and exergy. One can observe in Fig. 5 that with the increase in mass flow rate over the condensing cover the yield decreases as the contact time period between water and condensing cover is less. Maximum yield of 37.9 kg for case (III) is obtained in the month of June and minimum 17.18 kg for case (II) for the month of January (Fig. 5), at the mass flow rate over condensing cover of 0.025 kg/s. Thus, the mass flow rate of 0.025 kg/s is optimized for the three cases (I–III). Moreover, the effect of length of heat exchanger over the daily yield (kg) with different mass flow rates ($\dot{m}_f$)(kg/s) varying from 0.01 to 0.07 kg/s for the optimized thermal collector (Table 5) is studied from Fig. 6a–c. The graphs show the results as expected, i.e., the daily yield increases with the length of heat exchanger with the mass flow rate varying from 0.01 to 0.07 kg/s for all the cases (I–III) for the months of June and January, respectively. The reason is that as the length of heat exchanger increases from 0.5 to 1.97 m higher heat transfer occurs from fluid (inside the heat exchanger) to brackish water mass in the basin. The optimization of higher mass flow rate of water over condensing cover is less desirable as it lowers the exergy of the system. Therefore, a specific mass flow rate in thermal collector and over cooling condensing cover is studied and optimized for higher energy and exergy. At optimized conditions for the three active distillation systems cases (I–III), (Table 5) maximum yield obtained from case (I) is 35.9 and 34.1 kg, case (II) is 25.8 and 17.2 kg, and case (III) is 37.9 and 36.6 kg for the months of June and January, respectively.

The yield ($\dot{m}_{ew}$) obtained from the proposed system case (I) (without heat exchanger (L)) for the month of June is 14.8% higher than Singh and Tiwari [35]. Because the latent heat of condensation released after condensation of water vapor at the inner condensing cover is absorbed by the flowing water over the outer glass cover, which enhances the condensation and evaporation process. This results in enhancement of the yield (distilled water).

Case (B) Hourly and daily performance analysis on the bases of energy and exergy

On the bases of the above optimized parameters, hourly and daily performances for the three cases (I–III) have been studied. Daily yield (kg) (Eq. 21) and thermal exergy (kWh) (Eq. 22) for three cases (I–III) is calculated for the months of June and January, and the results are shown in Fig. 7. Case (III) shows maximum yield 37.9 kg and maximum exergy 2.54 kWh for the month of June for a particular day. It was observed that the increase in yield simultaneously reduces exergy as the entropy (thermal losses) is generated. Thus, optimization of system parameters is done for maximizing energy and exergy. Case (I) gives 8% higher yield for the

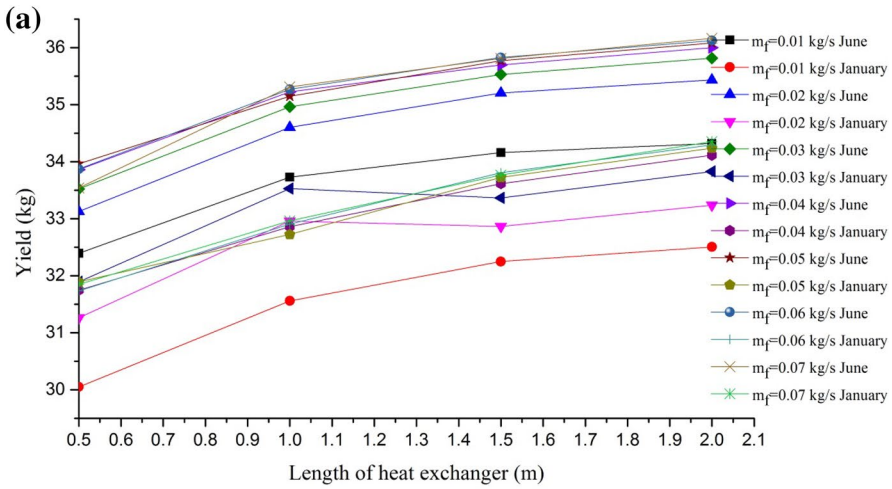

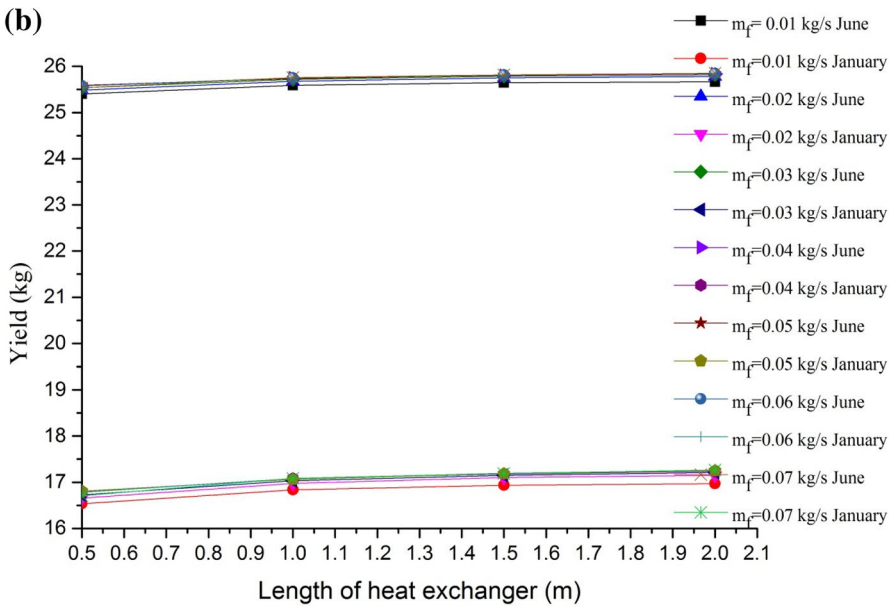

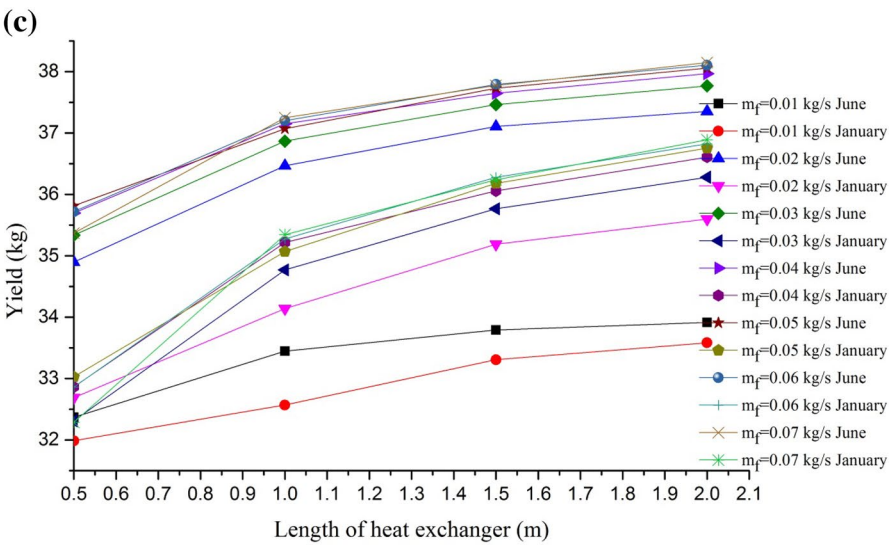

Fig. 6 **a** Variation of yield with length of heat exchanger at different mass flow rate for case (I) for the months of January and June, respectively. **b** Variation of yield with length of heat exchanger at different mass flow rate for case (II) for the months of January and June, respectively. **c** Variation of yield with length of heat exchanger at different mass flow rate for case (III) for the months of January and June, respectively

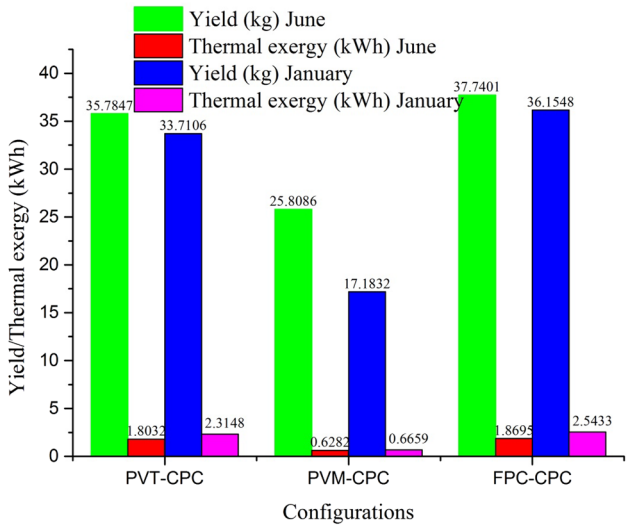

Fig. 7 Daily yield and thermal exergy for three cases (I–III) for the months of June and January, respectively

month of June compared to January and 36% higher exergy in the month of January because of the above mentioned reason. Similarly, case (II) and case (III) give 37 and 4% higher yield and 18.5 and 68% higher exergy in the month of June and January, respectively.

For cases (I) and (II), DC electrical energy is generated from semitransparent photovoltaic module from which, approximately 20 W is consumed in DC motor and further remaining power can be commercialized. The electrical efficiency (η_m) (Eq. 20) of solar modules decreases when there is rise in temperature of solar cells; if the thermal energy generated by solar cells is extracted it will result in increased electrical efficiency of module and lowers the probability of degradation of solar cell by thermal heating. Former, behavior of solar photovoltaic modules is observed in Fig. 8, and the latter is observed in Fig. 9, where the case (II) gives highest electrical efficiency of 13% for the month of January corresponding to minimum solar cell (η_m) temperature of 53 °C because of cooling condensing cover. Similarly, minimum electrical efficiency is obtained from case (I) for the month of June is 11%, corresponding to 75.69 °C of solar cell temperature (T_{cN}). The increased electrical efficiency (η_m) analogous to lesser cell temperature (T_{cN}) is obtained because a constant water mass of 0.025 kg/s flowing above the condensing cover (T_{go}) extracts the dissipated thermal heat from the outer glass cover (T_{go}), enhancing evaporation and simultaneously transfer of heat from the heat exchanger

Fig. 8 Hourly variation of cell temperature and module efficiency for case (I) and case (II) for the months of June and January, respectively

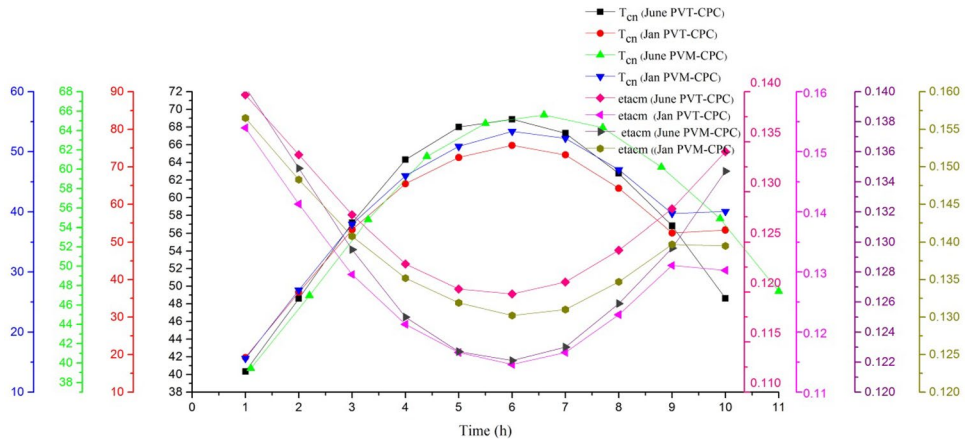

Fig. 9 Variation of cell temperature and module efficiency for case (I) and case (II) with mass flow rate flowing over the condensing cover for the months of June and January, respectively

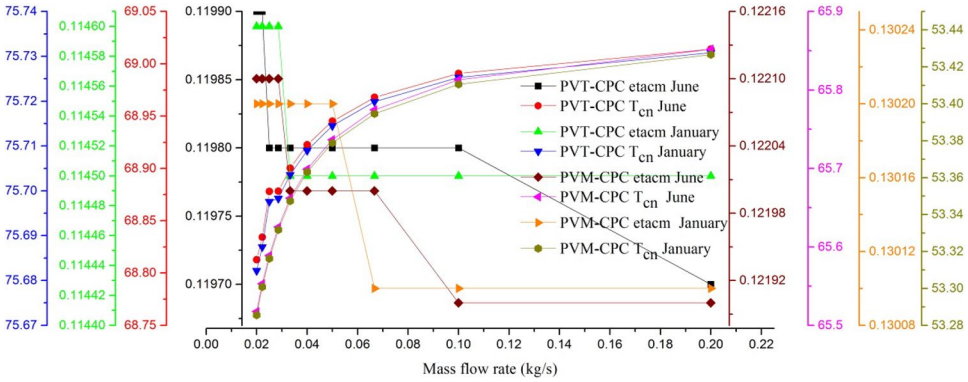

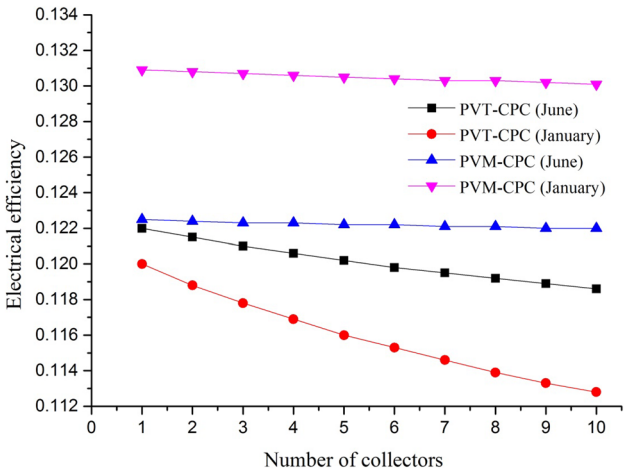

Fig. 10 Variation of electrical efficiency with number of collectors for case (I) and case (II) for the months of January and June, respectively

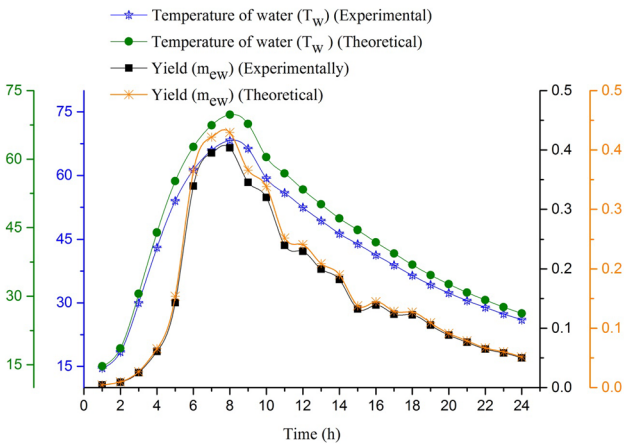

Fig. 11 Variation of water temperature and yield obtained from PVT-FPC-SS-SS

to water mass in the basin, thus higher thermal energy is extracted from thermal collectors which comprise photovoltaic modules as well. As a result, photovoltaic modules are cooled, giving higher electrical efficiency. This effect occurs in two active solar distillation systems case (I) and case (II) (Fig. 9). The decreasing electrical efficiency (η_m) curve with increasing solar cell temperature (°C) curve at higher mass flow rate of water ($\dot{m}_{fl}$) also confirms the reason that at higher mass flow rate as the contact time period is less, which lowers module efficiency and yield. The numerical values obtained in Fig. 9 are similar to the values obtained in Fig. 8.

The decreasing electrical efficiency behavior with the increase in the number of collectors is represented in Fig. 10. The fluid (water) flowing beneath the first semitransparent photovoltaic in thermal collectors Type (a, b) is at lower temperature thus, more electrical efficiency is obtained.

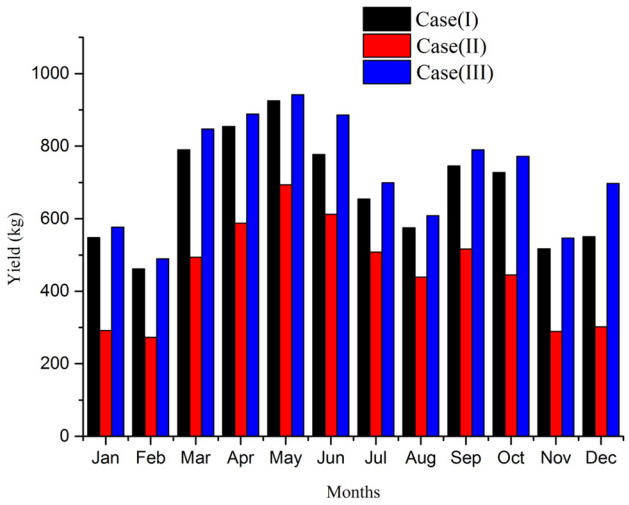

Fig. 12 Monthly variation of yield (distilled water) for three cases (I–III)

In consecutive thermal collectors, the fluid temperature is slightly higher than the previous ones, which lead to reduced electrical efficiency as higher temperature of water will extract lesser thermal energy liberated from solar cells. The maximum electrical efficiency obtained from Type (b) from single semitransparent photovoltaic module in the month of January is 13% and it decreases gradually with ten photovoltaic thermal collectors. Similar behavior is observed with Type (a) for the months of both June and January, respectively. Figure 11 shows the comparison of theoretical and experimental work done for the PVT-FPC-SS-SS (special case). The maximum temperature of water (T_w) obtained from theoretical/predicted work is 69.74 °C and from the experimental work is 68.26 °C. Similarly, yield is maximum around 3:00 p:m for both experimental and theoretical works, i.e., 0.4038 and 0.4295 kg.

The comparison of daily thermal energy (kWh), overall thermal energy (kWh), overall exergy (kWh), and collector exergy (kWh) for the three cases (I–III) is represented in Table 6 for the months of June and January. Higher thermal energy (kWh) leads to higher yield thus, case (III) is 15.5%, 10.2%, and 57.6%, 133% higher in the month of June and January, respectively, in comparison to case (I) and case (II). The overall thermal energy (kWh) is highest for case (II), i.e., 39.84 as the electrical gain is higher because of 10 fully covered photovoltaic thermal collectors, for the month of January. A percentage increase of overall thermal energy in case (II) is 13%, 38% higher than case (I) and 19%, 52% higher than case (III) for the months of June and January, respectively. The overall thermal exergy (kWh) for case (II) is maximum, i.e., 11.44 kWh and minimum for case (III), i.e., 1.86 kWh for the months of January and June, respectively. Collector exergy calculated in case (I) and case (III) shows that exergy in case

(III) is 15.43%, 15.26% higher from case (I) as expected, for the months of June and January, respectively.

Case (C) Monthly performance analysis on the bases of energy and exergy

Extending the values obtained from the daily basis to annual basis for the three cases (I–III), an annual yield (Fig. 12), overall thermal energy, overall thermal exergy, electrical energy, and solar radiation acts as input for the calculation of energy matrices, production cost of water and electricity, and co-generation efficiency. Energy matrices calculated on the bases of energy and exergy are represented in Table 7 for three active solar still cases (I–III). The energy payback time follows the order $(\text{EPBT})_{\text{case (III)}} < (\text{EPBT})_{\text{case (I)}} < (\text{EPBT})_{\text{case (II)}}$. Case (III) shows minimum energy payback time of 1 year because its embodied energy (kWh) is minimum (Table 8) and yield (Table 7) is maximum. The value of EPBT on the basis of exergy is lowest for case (II) (10 years) because higher electrical exergy is obtained from Type (b). Energy production factor (EPF) on the basis of energy is 57% higher in case (I) than case (II) and 24% lesser than case (III). Moreover, on the basis of exergy case (II) is 50% higher than case (I) and 125% higher than case (III). Life cycle conversion efficiency (LCCE) is highest for case (III) on the basis of energy as embodied energy is 26% lesser than case (I) and 61% lesser than case (II). Similarly, on the basis of exergy, LCCE is highest for case (II).

Case (D) Production cost of water and electricity, and co-generation efficiency for three cases (I–III)

The calculation of the capital investment (P), uniform end-of-year annual cost (UAC), and production cost of water (C_{wp}) and electricity (C_{e}) (Eq. 27) for the three cases (I–III) is represented in Tables 9, 10, and 11. Table 9 represents the cost of various components in (₹) utilized in the three hybrid solar distillation systems. Total capital investment of three cases (I–III) is ₹ 1,08,743, ₹ 1,94,993, and ₹ 90,743. Case (II) has a higher investment cost because of the higher number of fully covered photovoltaic thermal-compound parabolic concentrators (Table 5). The production cost of distilled water obtained from three cases (I–III) varies from Rs 0.11 to ₹ 2.12/kg. Case (i) gives a minimum production cost of water, i.e., ₹ 0.11/kg at 2% rate of interest which is 78% lesser than Singh and Tiwari [36] because the yield is higher and UAC is lower for the optimized parameters (Table 5) thus, system gets economically viable. The electricity generated in case (II), i.e., 1582 kWh, whereas distilled water obtained is 5451 kg. Thus, the hybrid active solar still [cases (II)] is sustainable from distillation point of view as production cost of electricity (C_{e}) is null, which means the production cost of water (C_{wp}) itself is capable of overcoming the total cost (UAC) of the system. Case (III) gives a production cost of water 190% higher than case (I) at a 2% rate of interest thus, it is less desirable. An interest rate of 5 or 10% gives the higher value of the production cost of water and electricity compared to 2%. The co-generation efficiency for the two cases (I) and (II) is represented in Table 12. The co-generation efficiency is 83% higher in case (I) compared to case (II) as electrical energy and thermal energy (yield) both are obtained in case (I), and the input solar radiation is 18% lesser for the life time of 50 years compared to case (II).

Conclusions

The following summarized conclusions have been drawn from the present study:

1. The optimum mass flow rates for the thermal collectors and water above condensing cover (T_{go}) are 0.04 and 0.025 kg/s for 1.97 m length of heat exchanger and 280 kg mass of water in basin for maximum energy and exergy of the three active solar distillation systems. The optimized numbers of thermal collectors are 6, 8, and 5 for the month of June and 7, 10, and 6 for the month of January for the three cases, respectively.
2. On the bases of overall thermal energy, daily electrical efficiency, energy payback time, production cost of water and electricity, and co-generation efficiency case (I) gives better results than case (II) and case (III).
3. In case (III) thermal energy, overall thermal exergy and collector exergy is higher and capital investment, uniform annual end-of-year annual cost (UAC) is lower.
4. Case (I), with cooling condensing cover is proposed for domestic and industrial purposes over case (II) and case (III), as it fulfills the commercial purposes such as charging of batteries, cleaning of medical equipment, avoiding scaling in equipments, and giving higher distilled water and electrical energy (direct current).

Acknowledgements The authors acknowledge the Department of Science and Technology (DST), Indian Institute of Technology-Delhi (IIT-D) for the financial help during the research work. We would also like to express our gratitude to the researchers who helped in the preparation of this manuscript.

Compliance with ethical standards

Conflict of interest On behalf of all the authors, the corresponding author states that there is no conflict of interest.

Appendix

$$Z_1 = \left(\propto_c \beta_c \tau_g \rho \frac{A_{am}}{A_{rm}}\right);$$

$$Z_2 = \frac{U_{tcp}}{(U_{L2} + (F' h_{pf}))}\left\{(\alpha\tau)_{2,eff} + PF_1 \alpha_c \beta_c \tau_g \rho \frac{A_{am}}{A_{rm}}\right\}$$

$$Z_3 = \frac{U_{tcp}((F' h_{pf}) + U_{tpf})}{2(\dot{m}_f C_f (U_{L2} + (F' h_{pf})))};$$

$$Z_4 = (PF_2(\alpha\tau)_{2,eff}) + \left(PF_1 PF_2 \alpha_c \beta_c \tau_g \rho \frac{A_{am}}{A_{rm}}\right) A_{rm} F_{rm}$$

$$Z_5 = \frac{U_{tcp}(F' h_{pf} + U_{tpf})}{2(\dot{m}_f C_f (U_{L2} + (F' h_{pf})))}; \quad Z_6 = PF_c (A_{rc} F_{rc})(\alpha\tau)_{c,eff}$$

$$Z_7 = (PF_2(\alpha\tau)_{2,eff}) + \left(PF_2 PF_1 \alpha_c \tau_g \beta_c \rho \frac{A_{am}}{A_{rm}}\right) A_{rm} F_{rm}\left(1 - \frac{A_{rc} F_{rc} U_{LC}}{\dot{m}_f C_f}\right)$$

$$Z_8 = (1 + K_m)\frac{\left(1 - K_K^{N-1}\right)}{1 - K_K};$$

$$Z_a = \left[(Z1 + Z2) + (Z_3 Z_4) + Z_5[\{Z_6 + Z_7\} Z_8]\right]$$

$$T_{a1} = \frac{U_{tcp}\left(\left(F' h_{pf}\right) + U_{tpf}\right)}{2\dot{m}_f C_f \left(U_{L2} + \left(F' h_{pf}\right)\right)};$$

$$T_{a2} = \left(AF_R U_L\right)_{m1} + \left(\left(AF_R U_L\right)_1 \frac{\left(1 - K_K^{N-1}\right)}{\left(1 - K_K\right)}\left(1 + K_m\right)\right)$$

$$Z_b = \left[\frac{U_{tcp}\left(F' h_{pf} + U_{tpf}\right)\left(1 + K_m\right) K_K^{N-1}}{2\left(U_{L2} + F' h_{pf}\right)}\right];$$

$$Z_9 = \tau_g \beta_c \rho \frac{A_{am}}{A_{rm}}; \quad Z_{10} = \frac{U_{tcp}}{\left(U_{L2} + \left(F' h_{pf}\right)\right)} PF_1 \tau_g \beta_c \rho \frac{A_{am}}{A_{rm}}$$

$$Z_{11} = \frac{U_{tcp}\left(F' h_{pf} + U_{tpf}\right)}{2\dot{m}_f C_f \left(U_{L2} + F' h_{pf}\right)} PF_1 PF_2 \tau_g \beta_c \frac{A_{am}}{A_{rm}} \rho A_{rm} F_{rm};$$

$$Z_{12} = \frac{U_{tcp}\left(F' h_{pf} + U_{tpf}\right)}{2\dot{m}_f C_f \left(U_{L2} + F' h_{pf}\right)}$$

$$Z_{13} = PF_1 PF_2 \tau_g \beta_c \rho \frac{A_{am}}{A_{rm}} A_{rm} F_{rm};$$

$$Z_{14} = \left(1 + \left(1 - \frac{A_{rc} F_{rc} U_{LC}}{\dot{m}_f C_f}\right)\right); \quad Z_{15} = (1 + K_m)\left(\frac{1 - K_K^{N-1}}{1 - K_K}\right)$$

$$Z_c = \left[Z_9 + Z_{10} + Z_{11} + (Z_{12} Z_{13} Z_{14})\right]$$

$$(\alpha\tau)_{1,eff} = \left(\rho \alpha_c \beta_c \tau_g - \eta_m \rho\right)\frac{A_{am}}{A_{rm}}; \quad (\alpha\tau)_{2,eff} = \rho \alpha_p \tau_g^2 (1 - \beta_c)\frac{A_{am}}{A_{rm}}$$

$$(\alpha\tau)_{m,eff} = (\alpha\tau)_{2,eff} + PF_1 (\alpha\tau)_{1,eff};$$

$$(\alpha\tau)_{c,eff} = \tau_g \alpha_p \rho \frac{A_{ac}}{A_{rc}}; \quad U_{L2} = U_{L1} + U_{tpf}$$

$$U_{Lm} = \frac{h_{pf} U_{L1}}{U_{L1} + F' h_{pf} + U_{tpf}}; \quad U_{Lc} = \frac{h_{pf} U_{tpa}}{F' h_{pf} + U_{tpa}};$$

$$PF_1 = \frac{U_{tcp}}{U_{tca} + U_{tcp}}; \quad PF_2 = \frac{h_{pf}}{U_{L1} + F' h_{pf} + U_{tpf}}$$

$$PF_c = \frac{h_{pf}}{F' h_{pf} + U_{tpa}}; \quad F_{rc} = \frac{\dot{m}_f C_f}{A_{rc} U_{Lc}}\left(1 - \exp\left(\frac{-\left(F' U_{Lc} A_{rc}\right)}{\dot{m}_f C_f}\right)\right);$$

$$F_{rm} = \frac{\dot{m}_f C_f}{A_{rm} U_{Lm}}\left(1 - \exp\left(\frac{-\left(F' U_{Lm} A_{rm}\right)}{\dot{m}_f C_f}\right)\right)$$

$$(AF_R(\alpha\tau))_1 = \left[\left(PF_c (\alpha\tau)_{c,eff} A_{rc} F_{rc}\right) + \left(PF_2 (\alpha\tau)_{m,eff} A_{rm} F_{rm}\left(1 - \frac{A_{rc} U_{Lc} F_{rc}}{\dot{m}_f C_f}\right)\right)\right]$$

$$\left(AF_R U_L\right)_1 = \left(A_{rc} F_{rc} U_{Lc}\right) + A_{rm} U_{Lm} F_{rm}\left(1 - \frac{A_{rc} U_{Lc} F_{rc}}{\dot{m}_f C_f}\right)$$

$$U_{tca} = \left[\frac{1}{h_o} + \frac{L_g}{K_g}\right]^{-1}; \quad U_{tcp} = \left[\frac{1}{h_i} + \frac{L_g}{K_g}\right]^{-1};$$

$$U_{tpf} = \left[\frac{L_g}{K_g} + \frac{1}{h_{pf}}\right]^{-1}; \quad U_{L1} = \frac{U_{tcp} U_{tca}}{U_{tcp} + U_{tca}}$$

$$K_m = 1 - \frac{A_{rm} F_{rm} U_{Lm}}{\dot{m}_f C_f}; \quad K_K = 1 - \frac{\left(AF_R U_L\right)_1}{\dot{m}_f C_f};$$

$$\left(AF_R U_L\right)_{m1} = A_{rm} F_{rm} U_{Lm}$$

$$T = \alpha_w I(t) + \frac{h_{bw} \alpha_b I(t)}{h_{bw} + h_{ba}} + U_{bca} T_a; \quad W = \frac{h_2 A_b h_{kg} A_g}{h_{kg} A_g + h_2 A_b};$$

$$Y = \frac{h_1 A_g}{h_1 A_g + (UA)_{wgo}}$$

$$Z = \frac{I(t)_3 + h_o T_a}{(UA)_{w,wf} + h_o}\left(1 - \frac{1 - \exp(-a_2 l)}{a_2 l}\right);$$

$$U1 = T_{wfi}\left(\frac{1 - \exp(-a_2 l)}{a_2 l}\right); \quad V = \frac{I(t)_A}{h_1 A_g + (UA)_{wgo}}$$

$$X = \frac{h_2 A_b \alpha_b I(t) A_g}{h_2 A_b + h_{kg} A_g}; \quad I(t)_A = \frac{h_{kg} A_g \alpha_g I(t) A_g}{h_{kg} A_g + h_2 A_b};$$

$$UA_{wgo} = \frac{h_{kg} A_g h_2 A_b}{h_{kg} A_g + h_2 A_b}; \quad UA_{w,wf} = \frac{h_1 (UA)_{wgo}}{h_1 A_b + (UA)_{wgo}}$$

$$h_{rw} = \varepsilon\sigma\left[\frac{(T_w + 273)^4 - (T_a - 273)^4}{(T_w - T_a)}\right];$$

$$h_{ew} = \left(16.27 \times 10^{-3} \times h_{cw} \times \left(\frac{P_w - P_a}{T_w - T_a}\right)\right)$$

$$h_{cw} = 0.884 \times \left[(T_{wfi} - T_a) + \frac{(P_w - P_a) \times (T_a + 273)}{(263.9 \times 10^3) - P_w}\right].$$

References

1. Addams, L., Boccaletti, G., Kerlin, M., Stuchtey, M.: WRG (Water resource group): Charting our water future—economic framework to inform decision-making. Mc Kinsey & Company, New York, Washington, DC (2009)
2. Della Porta, G.B.: Magiae Naturalis, Libri XX, Napoli (Italian translation, 1677, Napoli), English translation, New York, 1957, 1958, 1589 German translation, Nuremberg, 1713
3. El Sebaii, A.A.: Effect of wind speed on active and passive solar stills. Energy. Convers. Manag. **45**, 1187–1204 (2004)
4. Tiwari, A.K., Tiwari, G.N.: Thermal modeling based on solar fraction and experimental study of the annual and seasonal performance of a single slope passive solar still: the effect of water depths. Desalination **207**, 184–204 (2007)
5. Kabeel, A.E., Abdelgaied, M., Mahgoub, M.: The performance of a modified solar still using hot air injection and PCM. Desalination **379**, 102–107 (2016)
6. Shanmugan, S., Rajamohan, P., Mutharasu, D.: Performance study on an acrylic mirror boosted solar distillation unit utilizing seawater. Desalination **230**, 281–287 (2008)
7. Gupta, B., Shankara, P., Sharma, R., Baredar, P.: Performance enhancement using nano particles in modified passive solar still. Procedia Technol. **25**, 1209–1216 (2016)
8. Abdelal, N., Taamneh, Y.: Enhancement of pyramid solar still productivity using absorber plates made of carbon fiber/CNT-modified epoxy composites. Desalination **419**, 117–124 (2017)
9. Coventry, J.S.: Performance of a concentrating photovoltaic/thermal solar collector. Sol. Energy **78**, 211–222 (2005)
10. Proell, M., Osgyan, P., Karrer, H., Brabec, C.J.: Experimental efficiency of a low concentrating CPC PVT flat plate collector. Sol. Energy **147**, 463–469 (2017)
11. Rajaseenivasan, T., Raja, P.N., Srithar, K.: An experimental investigation on a solar still with an integrated flat plate collector. Desalination **347**, 131–137 (2014)
12. Gaur, M.K., Tiwari, G.N.: Optimization of number of collectors for integrated PV/T hybrid active solar still. Appl. Energy **87**, 1763–1772 (2010)
13. Arunkumar, T., Velraj, R., Denkenberger, D.C., Sathyamurthy, R., Kumar, K.V., Ahsan, A.: Productivity enhancements of compound parabolic concentrator tubular solar stills. Renew. Energy **88**, 391–400 (2016)
14. Sharshir, S.W., Peng, G., Wu, L., Yang, N., Essa, F.A., Elsheikh, A.H., Mohamed, S.I.T., Kabeel, A.E.: Enhancing the solar still performance using nanofluids and glass cover cooling: experimental study. Appl. Therm. Eng. **113**, 684–693 (2017)
15. Bassam, A.K.A.H.: Enhanced solar still performance using water film cooling of the glass cover. Desalination **107**, 235–244 (1996)
16. Dhiman, N.K., Tiwari, G.N.: Effect of water flowing over the glass cover of a multi wick solar still. Energy Converg. Manag. **30**, 245–250 (1990)
17. El-Samadony, Y.A.F., Kabeel, A.E.: Theoretical estimation of the optimum glass cover water film cooling parameters combinations of a stepped solar still. Energy **68**, 744–750 (2014)
18. Sahota, L., Shyam, Tiwari, G.N.: Energy matrices, enviroeconomic and exergoeconomic analysis of passive double slope solar still with water based nanofluids. Desalination **409**, 66–79 (2017)
19. Tiwari, G.N.: Enhancement of daily yield in a double basin solar still. Energy Conserv. Manag. **25**(1), 49–50 (1985)
20. Elango, T., Murugavel, K.K.: The effect of water depth on the productivity for single and double basin slope glass solar still. Desalination **359**, 82–91 (2015)
21. Pal, P., Yadav, P., Dev, R., Singh, D.: Performance analysis of modified basin type double slope multi-wick solar still. Desalination **422**, 68–82 (2017)
22. Murugavel, K.K., Srithar, K.: Performance study on basin type double slope solar still with different wick materials and minimum mass of water. Renew. Energy **36**, 612–620 (2011)
23. Sulttani, A.O.A., Ahsan, A., Rahman, A., Daud, N.N.N., Idrus, S.: Heat transfer coefficients and yield analysis of a double-slope solar still hybrid with rubber scrapers: an experimental and theoretical study. Desalination **407**, 61–74 (2017)
24. Morad, M.M., El-Maghawry, H.A.M., Wasfy, K.I.: Improving the double slope solar still performance by using flat-plate solar collector and cooling glass cover. Desalination **373**, 1–9 (2015)
25. Tellez, M.C., Figueroa, I.P., Juarez, A.S., Zayas, J.L.F.: Experimental study on the air velocity effect on the efficiency and fresh water production in a forced convective double slope solar still. Appl. Therm. Eng. **75**, 1192–1200 (2015)
26. Singh, G., Kumar, S., Tiwari, G.N.: Design, fabrication and performance evaluation of hybrid photo-voltaic thermal (PVT) double slope active solar still. Desalination **277**, 399–406 (2011)
27. Rahbar, N., Gharaiianc, A., Rashidia, S.: Exergy and economic analysis for a double slope solar still equipped by thermoelectric heating modules—an experimental investigation. Desalination **420**, 106–113 (2017)
28. Singh, D.B., Tiwari, G.N.: Performance analysis of basin type solar stills integrated with N-identical photovoltaic thermal (PVT) compound parabolic concentrator (CPC) collectors: a comparative study. Sol. Energy **142**, 144–158 (2017)
29. Rabl, A.: Optical and thermal properties of compound parabolic concentrators (CPC). Sol. Energy **18**, 497–511 (1976)
30. Fernandez, J., Chargoy, N.: Multistage, indirectly heated solar still. Sol. Energy **44**(4), 215F (1990)
31. Kumar, S., Tiwari, G.N.: Estimation of internal heat transfer coefficients of a hybrid (PV/T active solar still. Sol. Energy **83**, 1656–1667 (2009)
32. Jafarkazemi, F., Ahmadifard, E.: Energetic and exergetic evaluation of flat plate solar flat plate collector and hot air. Renew. Energy **56**, 55–63 (2013)
33. Nag, P.K.: Basic and Applied Thermodynamics. Tata McGraw-Hill Education, New Delhi, India (2002)
34. Tiwari, G.N., Mishra, R.K.: Advanced Renewable energy sources. Royal Chemistry of Society, Cambridge (2012)

35. Kumar, S., Tiwari, G.N.: Life cycle cost analysis of single slope hybrid (PV/T) active solar still. Appl. Energy **86**, 1995–2004 (2009)
36. Onovwiona, H.I., Ugursal, V.I.: Residential cogeneration systems: review of the current technology. Renew. Sustain. Energy Rev. **10**, 389–431 (2006)
37. Tiwari, G.N.: Solar Energy—Fundamentals. Modelling and Applications. Narosa Publishing House, New-Delhi, India, Design (2002)